

3-21-2013

# Modeling Radioactive Decay Chains with Branching Fraction Uncertainties

Timothy M. Higley

Follow this and additional works at: <https://scholar.afit.edu/etd>

Part of the [Nuclear Commons](#)

---

## Recommended Citation

Higley, Timothy M., "Modeling Radioactive Decay Chains with Branching Fraction Uncertainties" (2013). *Theses and Dissertations*. 930.

<https://scholar.afit.edu/etd/930>

This Thesis is brought to you for free and open access by the Student Graduate Works at AFIT Scholar. It has been accepted for inclusion in Theses and Dissertations by an authorized administrator of AFIT Scholar. For more information, please contact [richard.mansfield@afit.edu](mailto:richard.mansfield@afit.edu).



**MODELING RADIOACTIVE DECAY CHAINS WITH BRANCHING  
FRACTION UNCERTAINTIES**

THESIS

Timothy M. Higley, Captain, USAF

AFIT-ENP-13-M-14

**DEPARTMENT OF THE AIR FORCE  
AIR UNIVERSITY**

***AIR FORCE INSTITUTE OF TECHNOLOGY***

---

**Wright-Patterson Air Force Base, Ohio**

**DISTRIBUTION STATEMENT A.**

**APPROVED FOR PUBLIC RELEASE; DISTRIBUTION IS UNLIMITED**

The views expressed in this thesis are those of the author and do not reflect the official policy or position of the United States Air Force, Department of Defense, or the United States Government.

AFIT-ENP-13-M-14

**MODELING RADIOACTIVE DECAY CHAINS WITH BRANCHING  
FRACTION UNCERTAINTIES**

THESIS

Presented to the Faculty

Department of Engineering Physics

Graduate School of Engineering and Management

Air Force Institute of Technology

Air University

Air Education and Training Command

In Partial Fulfillment of the Requirements for the  
Degree of Master of Science in Nuclear Engineering

Timothy M. Higley, B.S.

Captain, USAF

March 2013

**DISTRIBUTION STATEMENT A.**  
APPROVED FOR PUBLIC RELEASE; DISTRIBUTION IS UNLIMITED.

**MODELING RADIOACTIVE DECAY CHAINS WITH BRANCHING  
FRACTION UNCERTAINTIES**

Timothy M. Higley, B.S.  
Captain, USAF

Approved:

  
Kirk A. Mathews, PhD (Chairman)

7 Mar 2013  
Date

  
LTC Stephen R. McHale (Member)

7 Mar 2013  
Date

  
Major Benjamin J. Kowash (Member)

8 Mar 2013  
Date

## Abstract

This thesis is a parameter study of the effects of branching fraction uncertainty from nuclear decay on isotope quantities at later times. Development of how to calculate and accurately draw random samples of branching fractions is done. Overall effects as well as isotope quantity uncertainty distributions are also explored. Isotope quantities are calculated using exponential moments methods with transmutation matrices. Uncertainty from both half-lives and branching fractions is carried through these calculations by Monte Carlo methods. Results of the study show that uncertainty from branching fractions dominates most isotopes present from neutron fission after approximately one month. Another result is that only 20% of isotopes present at any given time have uncertainty from both half-lives and branching fractions that are of the same order of magnitude. The final program is both flexible in the number and type of isotopes it can input and output, as well as computationally efficient.

*Dedicated to God and my family,  
when it is all said and done they will always be there for me.*

## **Acknowledgments**

I would like to thank my advisor Dr. Mathews. His understanding of nuclear engineering, math, and the English language, as well as his ability to blend the three together amazes me. Because of this and his guidance this work was possible. I would also like to thank my other nuclear engineering professors, LTC McHale, Maj Kowash, Dr. Petrosky, Dr. McClory, and Dr. Burggraf, whose expertise has helped me realize my goal of becoming a nuclear engineer.

Timothy M. Higley



## Table of Contents

	Page
Abstract .....	iv
Acknowledgments .....	vi
Table of Contents .....	vii
List of Figures .....	ix
List of Tables .....	xi
I. Introduction .....	1
Motivation .....	1
Nuclear Decay .....	1
Half-life Uncertainty .....	1
Branching Fraction Uncertainty .....	2
Decay Example .....	2
Problem .....	4
Goal .....	4
Scope .....	5
Assumptions .....	5
II. Random Sampling of Branching Fractions .....	7
Bernoulli Distribution .....	7
Binomial Distribution .....	8
Beta Distribution .....	8
Categorical Distribution .....	12
Multinomial Distribution .....	12
Dirichlet Distribution .....	13
Sampling Beta and Dirichlet Distributions .....	18
III. Implementation .....	29
Code Design .....	29
Input Data .....	30
Isotope Data .....	34
Distribution Sampling .....	35
Output Statistics and Data .....	36
Verification .....	38

Performance .....	39
IV. Results and Analysis.....	41
Uncertainty Ratios.....	42
Branching Fraction Uncertainty ( $\phi$ ) Results .....	47
Limiting Quantity Fraction .....	50
Quantity Fraction Distributions .....	52
V. Conclusions.....	61
Potential Future Work .....	62
Appendix A: Design Diagram of Decay Program .....	64
Appendix B: Derivation of Standardized Beta pdf .....	65
Appendix C: Derivation of Beta pdf Inflection Points .....	67
Appendix D: Derivation of Inverting CDF for a line .....	68
Appendix E: Derivation of Standardized Beta pdf Relative Slope.....	70
Appendix F: Prioritized List of Model and Code Improvements .....	71
Bibliography .....	74

## List of Figures

	Page
Figure 1. Diagram of notional decay chains from two isotopes. ....	3
Figure 2. pdf of beta distributions showing difference in number of trials. The variance of the red curve is smaller than the blue because more trials were done and it has the same mode. ....	10
Figure 3. pdf of beta distributions with 100 trials but different number of successes. The difference in the parameters shows how the mode and the max value of the pdf are affected. ....	11
Figure 4. pdf of a Dirichlet distribution with concentration parameters (61, 31, 11), of which the second two parameters are shown. The peak is centered around $x_2 = 0.3$ and $x_3 = 0.1$ , which corresponds to the mode of the second two parameters (31, 11). ....	16
Figure 5. 3d plot of a Dirichlet pdf, with concentration parameters (301, 151, 51), of which the second two parameters are shown. The peak is centered at the same place as in Figure 4 because their modes are the same, but is much narrower because the sum of the parameters is greater. ....	17
Figure 6. $Beta_s(x; 50, 450)$ , orange and red lines are rejection sampling functions from 0 to the 1 <sup>st</sup> inflection point, and 2 <sup>nd</sup> inflection point to 1 respectively. Green line represents constant sampling function around the peak of $Beta_s$ . ....	24
Figure 7. $Beta_s(50, 450)$ , orange, and red lines represent the four linear rejection scheme. Green line represents constant sampling function around the peak of $Beta_s$ . ....	26
Figure 8. Comparison of uncertainty due to branching fractions ratios as a percent of all isotopes present for U238 high and $\varphi = 10\%$ . ....	44
Figure 9. Comparison of empirical CDFs for the different ratios at 1 second and ~1.5 years for U238 high and $\varphi = 10\%$ . At both times the ratio for most isotopes is either very close to zero or one. This means very few isotopes have uncertainties from both half-lives and branching fractions that are of the same order of magnitude. ....	45
Figure 10. Comparison of multiple uncertainty ratio values as a percent of all isotopes present for U238 high and $\varphi = 10\%$ . ....	46

Figure 11. Comparison of Branching Fraction Uncertainties ( $\varphi$ ) with ratio values of 0.5 as a percent of all isotopes present for U238 high.....	47
Figure 12. Empirical CDFs of the Ground State of Sn129 with different values of $\varphi$ from U235 thermal at 10,000 seconds.....	49
Figure 13. Limiting quantity fraction effect on percent of isotopes dominated by branching fraction uncertainty for U238 high fission and $\varphi = 10\%$ .....	51
Figure 14. Empirical CDFs of the Ground State of Sn129 from U235 thermal at 10,000 seconds with $\varphi = 1\%$ , as compared to a Normal CDFs with the same mean and standard deviation.....	53
Figure 15. Empirical CDFs of Te124 from Pu239 fast at 0.1 seconds with $\varphi = 20\%$ , as compared to a Normal CDFs with the same mean and standard deviation. ....	54
Figure 16. Log log plot of the quantity of Te124 as a function of time from Pu239 fast where $\varphi = 20\%$ . The error bars represent one standard deviation from the mean. ...	55
Figure 17. Empirical CDFs of the Xe139 from U238 fast after 100 seconds with $\varphi = 1\%$ , as compared to a Normal CDFs with the same mean and standard deviation.....	56
Figure 18. Log log plot of the quantity of Ni74 as a function of time for U235 fast fission with $\varphi = 5\%$ . The error bars represent one standard deviation from the mean.....	58
Figure 19. Empirical CDFs of Ni74 from U235 fast fission at 46.4 seconds with $\varphi = 5\%$ . .....	59
Figure 20. Empirical CDFs of Ni74 from U235 fast at 1 second with $\varphi = 5\%$ . ....	60
Figure 21. pdf of two Gaussians with different standard deviations spliced together. The mean is 0.5.....	72

## List of Tables

	Page
Table 1. Sample Nuclear Wallet Card output from the NuDat 2.6 database. ....	32
Table 2. Sample format for the initial isotope quantity input. ....	32
Table 3. Quantity standard deviation of Sn129 ground state for varying $\varphi$ at 10,000 seconds from U235 thermal fission. ....	50

# MODELING RADIOACTIVE DECAY CHAINS WITH BRANCHING FRACTION UNCERTAINTIES

## I. Introduction

### Motivation

A method of calculating radioactive decays with quantifiable uncertainty is desired to ensure the utility of measurements. It is important to know quantities of isotopes after a given time, to more accurately model nuclear fallout or trace what type and amount of nuclear material was present originally. Knowing the uncertainty that goes along with measurements taken ensures accurate conclusions are drawn. A key step in determining uncertainty is to identify its driving sources. The motivation behind this work is to identify whether one of these sources is branching fractions.

### Nuclear Decay

Decay chains of radioactive materials depend on three things, quantity of the isotopes initially present, half-lives of those isotopes, and the branching fractions of their decay. Given initial quantities of one or more isotopes, one can calculate what isotopes are present and their quantity at a later time. Knowing this information is valuable to understanding the environmental hazards that result from radioactive decay, or being able to accurately determine the quantities of isotopes present at earlier times.

### Half-life Uncertainty

Half-lives of radioactive materials span many orders of magnitude. Because of this, calculating the quantity of each isotope present in a decay chain after some period of

time becomes difficult. Different types of equilibrium may arise due to long lived isotopes decaying to short lived isotopes or vice versa. Because of this large range, half-life uncertainty can have a major effect on decay chains.

### **Branching Fraction Uncertainty**

If an isotope has more than one type of decay that results in multiple daughters, then the fraction of decays that result in each daughter are taken to be that isotope's branching fractions. The resulting daughters may or may not be radioactive, and their branching fractions can vary by orders of magnitudes. Each of these fractions has an uncertainty, and again because of the same reasons laid out for half-lives, this can have an effect on decay chains.

### **Decay Example**

To illustrate the effects of branching fraction uncertainty, consider Figure 1. It shows a notional diagram of two initial isotopes (A and B) and their decay chains. Under the name of each isotope is the time scale of its half-life. The only branching in these decay chains is in the initial decays, which is not always the case, but is illustrated here for simplicity. The percentages on the arrows for the decay represent the average branching fraction. Lastly it is assumed there are 100 moles of isotope A initially present and 10 moles of isotope B.

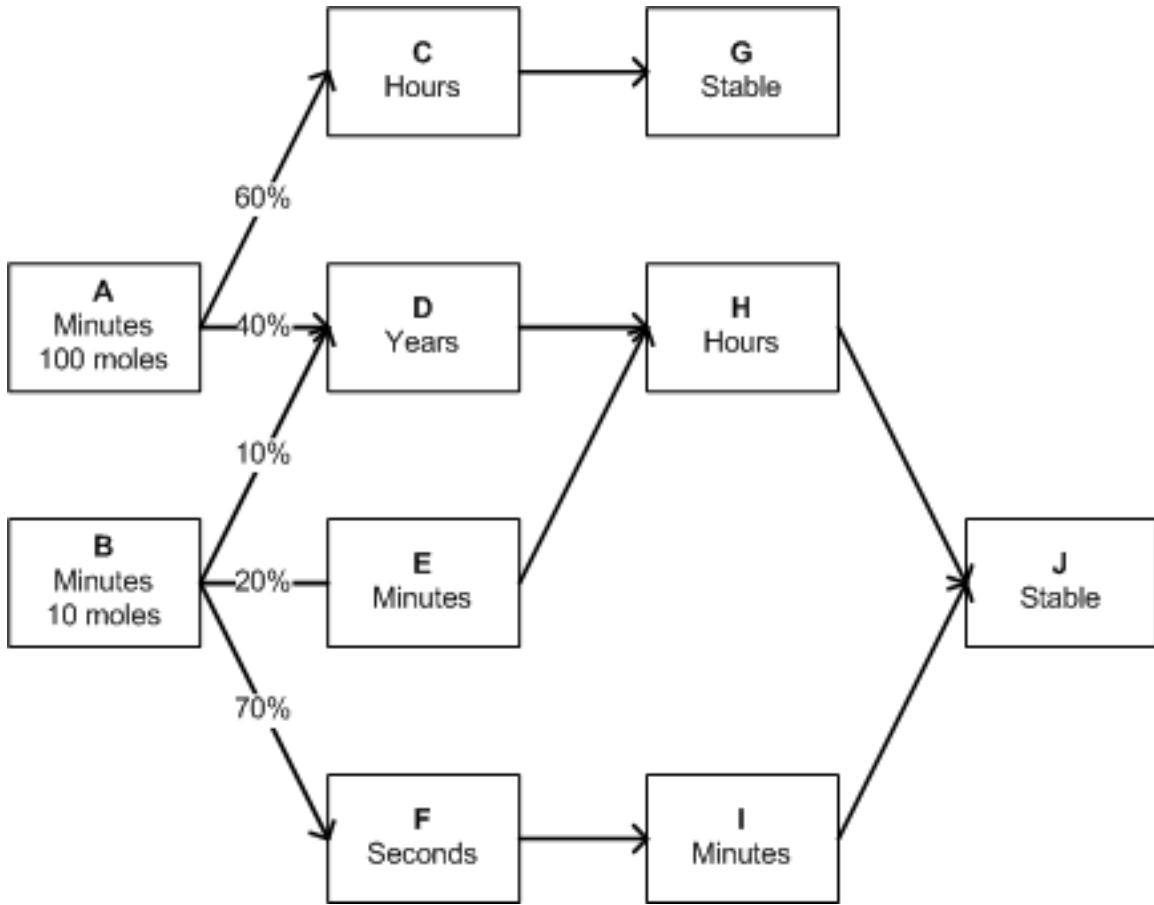


Figure 1. Diagram of notional decay chains from two isotopes.

Notice that all chains lead to either stable isotopes G or J, and all of B ultimately lead to J. With no branching fraction uncertainty, eventually all 10 moles from B and 40 moles from A would become J. The remaining 60 moles of A would become G. Regardless of half-life uncertainty, this would be the end result. During the time it takes for all these decays to occur, half-life uncertainty would have an effect on which isotopes were present at a given time. Now consider branching fraction uncertainty, and assume the 40% that goes from  $A \rightarrow D$  can vary by  $\pm 5\%$ . If 45 moles decayed to D instead of 40 the end result would be 55 moles of J, and 55 moles of G. This is a change of 10% in the



amount of J compared to when there was no branching fraction uncertainty. It not only has an effect on the end products, but it affects when an isotope may be present just like half-life uncertainty. Now consider the branch from  $B \rightarrow D$ . If two moles went to D, and only one went to E it changes how much and at what times H is present. This is due to the large difference in half-lives between D and E. Numerous scenarios can be explored just with this simple diagram. Try to imagine the complexity that results from having around 800 initial isotopes with thousands of decay chains. The potential effect of branching fraction uncertainty becomes clear.

### **Problem**

Model the time-dependent quantities of all known isotopes given an initial amount of isotopes present. Include the uncertainties of those quantities due to the half-life and branching fraction uncertainties of each individual isotope.

### **Goal**

The goal of this work is to understand how branching fraction uncertainties contribute to the overall uncertainty in the quantity of isotopes present at a given time. This is done by comparing or combining branching fraction uncertainties with the uncertainty from half-lives to get a sense of if and when it becomes a major source in quantity uncertainty. Quantification of these uncertainties will help interested organizations determine if experiments designed to measure branching fraction uncertainty are warranted and set priorities for said experiments.

## Scope

Because few of the branching fraction uncertainties are known, the scope of the project was to develop a tool to complete a parameter study. Incorporating existing branching fraction uncertainties was initially explored but was determined to be beyond the scope of this study. This was due to issues in weighting and incorporating these datasets and the fact that their distributions were probably quoted as normal when they are not. The program can read in isotope data including metastable states, half-life, branching fraction, and decay information. It will also take in any number of initial isotope quantity datasets. The output is quantity and basic statistics to evaluate uncertainty of any isotope including metastable states at any positive time.

## Assumptions

A consistent method of applying uncertainty is used, because a majority of the branching fraction uncertainties are unknown. For each isotope that has more than one type of decay associated with it, the branching fraction with the smallest mean is chosen. Its relative standard deviation (standard deviation divided by the mean or  $\sigma/\mu$ ) is assumed to be equal to a percentage. This same percentage is applied to the smallest fraction for all isotopes in a given run of the program, making the relative standard deviation of the smallest branching fraction a primary independent variable in the parameter study. Because the standard deviation of each branch of a given isotope is dependent on the others, knowing one allows you to calculate the others.

Another assumption is that there is no uncertainty in the initial amounts of the isotopes present. Eliminating this variable allowed the study to focus on branching

fraction uncertainty and how its effects compare with the effects from half-life uncertainty. This feature could be incorporated into the program for fission fragment yield uncertainties in the future because the same method used to draw random samples for branching fraction uncertainties applies.

## II. Random Sampling of Branching Fractions

The overall approach uses Monte Carlo methods to develop quantity uncertainties. For each Monte Carlo trial, a random sample from the uncertainty distributions for half-lives and branching fractions is drawn. This method was chosen over trying to carry these individual uncertainties through the differential equations that define their decay for its relative mathematical simplicity and computational efficiency.

The model used builds upon the work of Harr [1], who focused on half-life uncertainties, and their effect on the uncertainty of gamma activity. His use of the exponential moment methods, method for sampling from normal distributions for half-life uncertainty, and use of transmutation matrices were leveraged. This chapter discusses several distributions that will lead to an understanding of what is necessary to randomly sample branching fractions. It then develops a method for sampling these branching fractions, while avoiding biasing or catastrophic cancellation that can occur from normalizing.

### **Bernoulli Distribution**

The Bernoulli distribution is a discrete probability function with only two possible outcomes. Discrete meaning there is only success or failure for each trial. The best example of this is the flipping of a coin. The two possible outcomes are heads or tails. The probability for each outcome must be in  $(0, 1)$ , and the sum of the two probabilities must equal one. If we assume the probability is equal for both outcomes, then the probability for each trial and for both heads and tails is 0.5. If the coin has a probability

of 0.7 for heads then the probability for tails would be  $1 - 0.7 = 0.3$ . A Bernoulli distribution only considers one trial ( $n = 1$ ).

### **Binomial Distribution**

If more than one trial is done with the same parameters as the Bernoulli distribution, then it is a binomial distribution. If the probability for an outcome is known, then for a given number of trials the probability of getting any number of successes or failures can be calculated from the probability mass function (pmf). The pmf for a binomial is given as:

$$\text{Binomial pmf} = \frac{n!}{x!(n-x)!} p^x (1-p)^{n-x} \quad (1)$$

where  $n$  is the number of trials  $x$  is the number of successes and  $p$  is the probability of success. Consider the coin example again where the probability of success was 0.5 and now the number of trials is set at 100. There would be a 7.96% chance of getting exactly 50 successes, and a 1.08% chance of getting exactly 40 successes.

### **Beta Distribution**

Now assume the probability of success is unknown, and there are still only two possible outcomes. An experiment is done with  $n$  trials to determine the probability of success. It would make sense that the more trials that are done the more confidence there would be in this probability. This is known as a conjugate prior distribution, or taking the information that is known and building a distribution from it. The beta distribution is the conjugate prior of the binomial distribution, and whose probability density function (pdf) is:

$$\text{Beta}(x; \alpha, \beta) = \frac{x^{\alpha-1}(1-x)^{\beta-1}}{\int_0^1 t^{\alpha-1}(1-t)^{\beta-1} dt} = \frac{x^{\alpha-1}(1-x)^{\beta-1}}{B(\alpha, \beta)} \quad (2)$$

where  $\alpha$  and  $\beta$  are the concentration parameters of the distribution,  $0 \leq x \leq 1$ , and the denominator is the beta function  $B(\alpha, \beta)$ . As an example if no prior knowledge of the probability of success were known, and 100 trials were performed with 50 successes as the result. The beta pdf would have parameters  $\alpha = 51$  and  $\beta = 51$ , where  $\alpha$  is equal to one plus the number of successes and  $\beta$  is equal to the one plus the number of failures. The resulting pdf is shown in Figure 2 along with another beta pdf with parameters  $\alpha = 101$  and  $\beta = 101$ . While they make look Gaussian, they are not. What does make sense is that the highest probability of success is right at 0.5, because 1/2 of the trials performed turned out successful. What should also be noted is that when the number of trials was doubled to 200 the standard deviation decreased, and the probability at 0.5 increased. This too makes sense because you have twice as much information as in the first experiment, that supports that the probability is most likely 0.5.

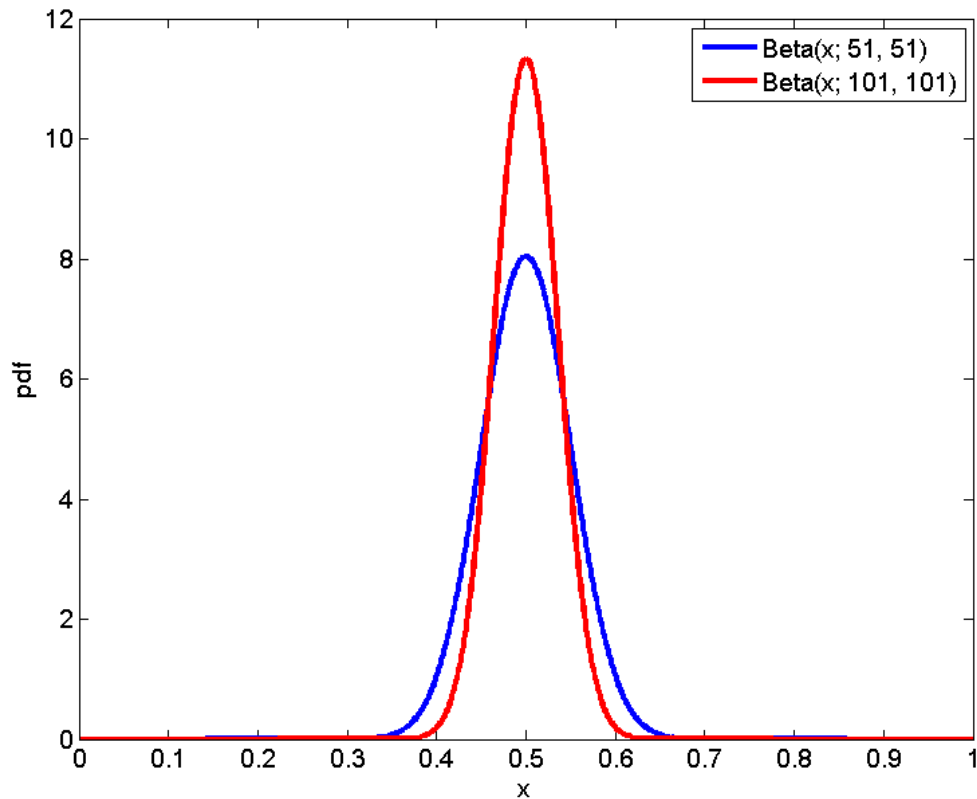


**Figure 2. pdf of beta distributions showing difference in number of trials. The variance of the red curve is smaller than the blue because more trials were done and it has the same mode.**

Now consider two other scenarios, both that have 100 trials but one has 65 successes and the other has only 5 successes. The resulting pdf distributions are shown in Figure 3. The pdf with 65 successes still looks rather Gaussian, but it has shifted to the right to show a higher probability of success around 0.6. The second distribution is very close to zero, and if is examined closely the right tail is larger than the left indicating it is not symmetric like a normal distribution.

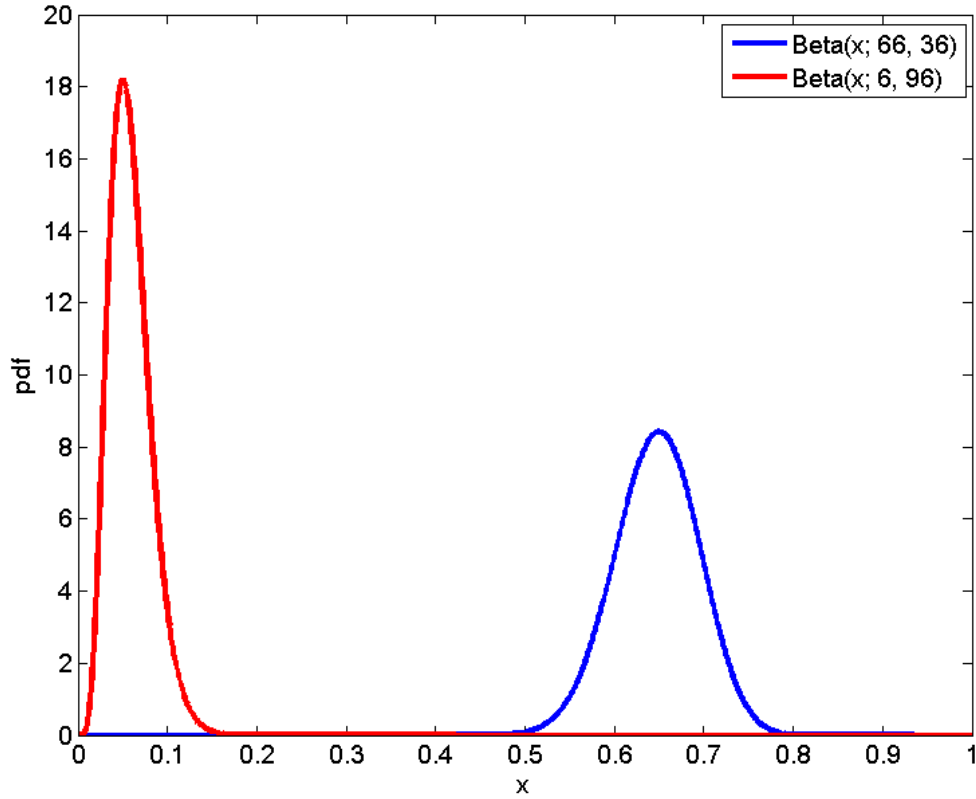


**Figure 3. pdf of beta distributions with 100 trials but different number of successes. The difference in the parameters shows how the mode and the max value of the pdf are affected.**

Branching fractions for each isotope without uncertainty are documented in the National Nuclear Data Center's NuDat 2.6 database [2]. It is assumed that these branching fractions are the means of the probabilities. However, to solve for both the  $\alpha$  and  $\beta$  parameters, the standard deviation or variance of one of the branches must be known. The mean and standard deviation of a beta distribution are:

$$\mu_{Beta} = \frac{\alpha}{\alpha + \beta}, \quad \sigma_{Beta} = \sqrt{\frac{\alpha\beta}{(\alpha + \beta)^2(\alpha + \beta + 1)}} \quad (3)$$



Of note is that, unlike a Gaussian, the mean of a beta is not the mode. The simplicity of these equations means its parameters can quickly be calculated. If the means of both branches and variance or standard deviation of one of the branches is known, then its  $\alpha$  and  $\beta$  can be calculated. The beta distribution can then be sampled from and the other branch is determined by taking one minus the sample drawn. This will not work for instances where the number of categories is greater than two, which require a different distribution.

These three types of distributions (Bernoulli, Binomial, and Beta) are based on only having two possible outcomes. Some isotopes can decay in more than two ways, so the generalization to these distributions that handle multiple possible outcomes is presented in the next sections.

### **Categorical Distribution**

The generalization of the Bernoulli distribution is the categorical distribution. A categorical distribution has  $j$  possible outcomes. The probability of each of those outcomes is known and they sum to one. As an example, isotope A decays to isotope B 60% of the time, isotope C 30% of the time, and D 10% of the time. This means that isotope B has a probability of 0.6, isotope C of 0.3, and isotope D 0.1 in the categorical distribution and they sum to exactly 1.

### **Multinomial Distribution**

The generalization of the binomial distribution is the multinomial distribution. As with the binomial, more than one trial is done and the probability of success for each

outcome is known. The pmf with the probabilities of getting a certain number of successes is:

$$\text{pmf}(x_1, x_2, \dots, x_j) = n! \prod_{i=1}^j \frac{p_i^{x_i}}{x_i!} \quad (4)$$

where  $n = \sum_{i=1}^j x_i$  is the number of trials,  $j$  is the number of categories,  $x_i$  are the number of successes for each category (which sum to  $n$ ), and  $p_i$  is the probability of success for each category (which sum to 1). Equation (4) is equal to the binomial pmf in Equation (1), when  $j = 2$ . This relates to radioactive decay. Assume there is no uncertainty in the branching fractions of isotope A from the previous example. The probability of seeing a certain number of isotope B, C, or D from a known number of decays of A could be calculated from the pmf. The problem is that the probabilities can never be known exactly; therefore, the conjugate prior to this distribution is needed. A conjugate prior distribution creates a pdf based on known data.

### **Dirichlet Distribution**

The Dirichlet distribution is the conjugate prior to the multinomial distribution and generalization of the beta distribution. The Dirichlet has  $j$  possible outcomes, takes known information and gives a pdf for each of those outcomes. The Dirichlet has  $j$  concentration parameters. Like the beta distribution each parameter is equal to one plus the number of successes witnessed. The pdf of the Dirichlet distribution is given in Equation (5).

$$\text{Dir}(x_1, x_2, \dots, x_j; \alpha_1, \alpha_2, \dots, \alpha_j) = \frac{\Gamma(\alpha_0)}{\prod_{i=1}^j \Gamma(\alpha_i)} \prod_{i=1}^j x_i^{\alpha_i-1} \quad (5)$$

$$\sum_{i=1}^j \alpha_i = \alpha_0 \quad \text{and} \quad \sum_{i=1}^j x_i = 1$$

where  $\alpha_i$  are the concentration parameters,  $x_i$  are the branching fractions in (0,1), and  $\Gamma$  is the gamma function. It can be shown that the Dirichlet is the generalization of the beta pdf in Equation (2) by setting  $j = 2$  in Equation (5) and using the property  $B(x, y) = \Gamma(x)\Gamma(y)/\Gamma(x + y)$ . Kotz [3] also proves that the marginal distributions of a Dirichlet are beta distributions. A marginal distribution is a distribution that defines the probability of a single or subset of the possible outcome(s). The beta distributions that represent the marginal distributions of a Dirichlet are:

$$\text{Beta}(x_i; \alpha_i, \alpha_0 - \alpha_i) \quad (6)$$

In order to sample each of these beta distributions, all concentration parameters of the Dirichlet must be known. Similar to a beta, the Dirichlet parameters can be calculated from the mean and standard deviation of each parameter, which is given in Equations (7), (8), and (9).

$$\text{Mean of } x_i = \mu_i = \frac{\alpha_i}{\alpha_0} \quad (7)$$

$$\text{Mode of } x_i = \frac{\alpha_i - 1}{\alpha_0 - j} \quad (8)$$

$$\text{Standard Deviation of } x_i = \sigma_i = \sqrt{\frac{\alpha_i(\alpha_0 - \alpha_i)}{\alpha_0^2(\alpha_0 + 1)}} \quad (9)$$

Just like a beta, the means are assumed to be the quoted branching fractions. A closer look shows the mean is a ratio of the individual concentration parameter to the sum of the

concentration parameters. In the case of interest, this is simply the branching fraction mean times a scalar. It also shows that the mode differs from the mean. Equation (9) reveals that as the sum of the concentration parameters increases the standard deviation decreases approximately inversely with  $\alpha_0$ . This means the size of the scalar (sum of the concentration parameters,  $\alpha_0$ ) determines the standard deviation of all the possibilities. If all the means are known and the variance or standard deviation of one of the branches is known, then the sum of concentration parameters can be calculated. This then determines the standard deviation of the other branches.

Now expand on the example used in the categorical distribution section. An experiment was done and it was measured that out of 100 decays 60 times it went to B, 30 times it went to C, and 10 times it went to D. The Dirichlet distribution would have concentration parameters of 61, 31, and 11. Using Equation (9) the standard deviation of the branch going to isotope B would be 0.0482. If the same experiment was done but this time 500 decays were measured and 300 times it went to isotope B then the standard deviation would be 0.0218. This makes sense because the counting statistics are better in the experiment with 500 measurements making the variance smaller.

This can be seen by looking at a 3d plot of our 100 measurement example Dirichlet distribution in Figure 4. The plot is the pdf which can only show two parameters at a time. Figure 4 shows the parameters 31 and 11 representing isotopes C and D respectively.

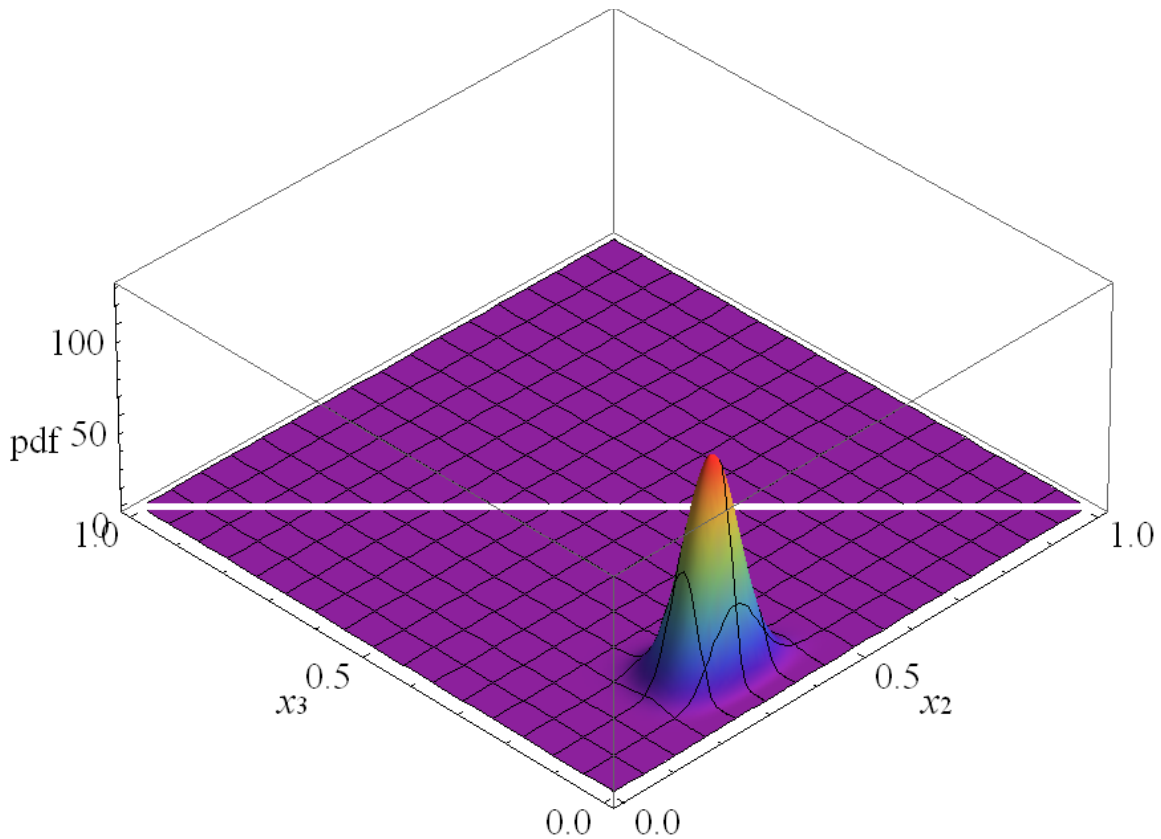


**Figure 4. pdf of a Dirichlet distribution with concentration parameters (61, 31, 11), of which the second two parameters are shown. The peak is centered around  $x_2 = 0.3$  and  $x_3 = 0.1$ , which corresponds to the mode of the second two parameters (31, 11).**

Figure 4 shows a single peak that is centered near 0.3 in the  $x_2$  direction, and 0.1 in the  $x_3$  direction. This corresponds to the means of the parameters 31 and 11 in the Dirichlet distribution (remember the mean is not where the peak is). The white line that cuts through the middle of the graph is a limit of possible value. That is, behind it those values are not possible in the distribution because the sum of the values must be equal to one. If the Dirichlet concentration parameters are changed to the experiment with 500 measurements the 3d plot would look like Figure 5.

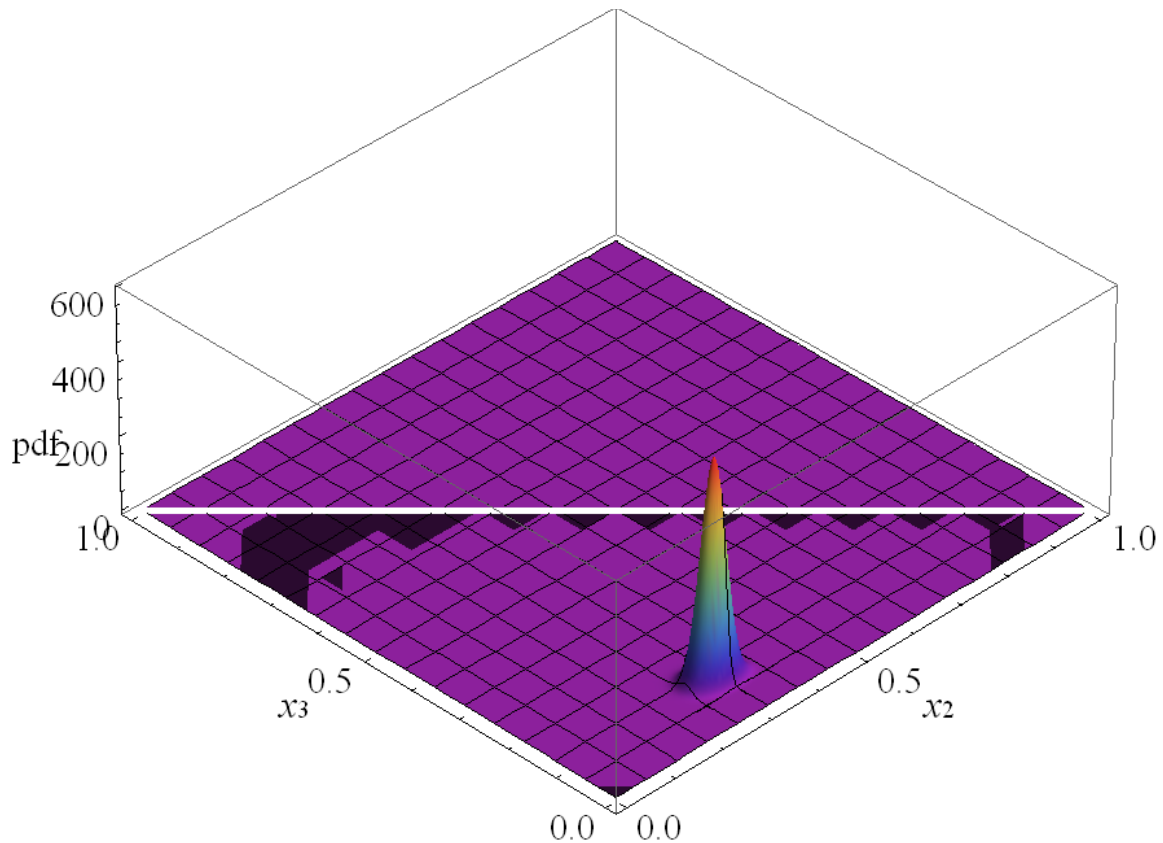


**Figure 5.** 3d plot of a Dirichlet pdf, with concentration parameters (301, 151, 51), of which the second two parameters are shown. The peak is centered at the same place as in Figure 4 because their modes are the same, but is much narrower because the sum of the parameters is greater.

The peak in Figure 5 is almost in the same exact location as Figure 4, but it is much narrower than Figure 4's. This is expected since the means of both distributions are the same, but the sum of the concentration parameters in Figure 5 is greater meaning the variances of each parameter are smaller, resulting in a narrower peak.

The beta and Dirichlet distributions look to be the best choice for randomly sampling branching fractions. This is because the distributions must be continuous on the interval of  $[0, 1]$ , and the probability be 0 at both 0 and 1. If the probability is not 0 at both 0 and 1, then an isotope could potentially eliminate itself or another isotope

(catastrophic cancellation). This eliminates the possibility of it being Gaussian, because it cannot have a probability equal to zero. A truncated Gaussian is not a realistic possibility either. This is because in order for the probability to be 0 at 0 and 1 the truncation would have to be at  $0 + \epsilon$  and  $1 - \epsilon$  ( $\epsilon$  – very small number or machine precision). This leaves a step value right at the boundaries that is not realistic. The beta and Dirichlet distributions are the most logical choices that satisfy the above requirements.

### Sampling Beta and Dirichlet Distributions

Having chosen the Dirichlet and beta distributions, an efficient method for drawing samples from these distributions is needed. This will start with determining the Dirichlet concentration parameters. This method will also work with isotopes that have only two branches or  $j = 2$ , since a Dirichlet is the generalization of a beta distribution.

Consider a Dirichlet distribution where  $\mu_1, \mu_2, \dots, \mu_j$  are the means of the branching fractions, and  $\alpha_0$  is the sum of the Dirichlet concentration parameters. From Equation (7) the individual concentration parameters ( $\alpha_i$ ) become:

$$\text{Dir}(\mu_1\alpha_0, \mu_2\alpha_0, \dots, \mu_j\alpha_0) \quad (10)$$

where  $\alpha_i = \mu_i\alpha_0$ ,  $0 < \mu_i < 1$ ,  $\sum_{i=1}^j \mu_i = 1$ , and  $\alpha_0 \geq 1$ . The standard deviation of each variable  $x_i$ , can also be calculated from Equation (9) to be:

$$\sigma_i = \sqrt{\frac{\mu_i(1 - \mu_i)}{\alpha_0 + 1}} \quad (11)$$

Now let  $s$  be the index of the branching fraction with the smallest mean, and  $\varphi$  be the relative standard deviation of that branch. Relative standard deviation, also called

coefficient of variation, is defined as the standard deviation divided by the mean ( $\sigma/\mu$ ). The smallest branch is chosen because it has the largest relative standard deviation making it the most sensitive parameter. Using this we can solve for  $\alpha_0$  in terms of  $\varphi$  and  $\mu_s$ .

$$\sqrt{\frac{\mu_s(1 - \mu_s)}{\alpha_0 + 1}} = \left(\frac{\sigma_s}{\mu_s}\right) \mu_s = \varphi \mu_s \quad (12)$$

Solve for  $\alpha_0$ :

$$\alpha_0 = \frac{1 - \mu_s - \varphi^2 \mu_s}{\varphi^2 \mu_s} = \frac{1}{\varphi^2} - 1 \quad (13)$$

once  $\alpha_0$  is known from Equation (13) each concentration parameter is calculated by multiplying its mean by  $\alpha_0$ . Once the concentration parameters are known they are checked to make sure none are greater than  $10^{15}$ . If a parameter is greater than  $10^{15}$  and its mean is close to one, the double precision random number will round to one because it does not have enough digits. When a parameter is greater than  $10^{15}$  its sample is simply its mean. In the current isotope input data no concentration parameters meet this criterion, but this was put in to prevent potential future errors. This issue can be put off by using greater precision at the cost of memory. Now each branch can be sampled from its marginal  $\text{Beta}(x_i; \alpha_i, \alpha_0 - \alpha_i)$ .

To maximize sampling efficiency, several beta distribution sampling and rejection schemes were explored. The first and easiest to implement was to use a geometric rejection scheme. The beta pdf is standardized to unity at its peak, which is developed in Appendix B, and referred to as  $\text{Beta}_S(x; a, b)$ . This means both  $x$  and  $\text{Beta}_S$  must be in  $(0,1)$ . A random number ( $\zeta_1$ ) is drawn and  $\text{Beta}_S(\zeta_1; a, b)$  is calculated. Then a second



random number ( $\zeta_2$ ) is drawn and if  $\zeta_2 \leq \text{Beta}_S(\zeta_1; a, b)$ , then  $\zeta_1$  is the used as the random sample, otherwise the process is repeated with two new random numbers. While simple, this method is not very efficient and parsimonious, especially if either beta distribution parameter is much less than the other.

The other scheme explored is called “Rejection using Random-Term Sampling” and is laid out by Mathews [4]. It uses a rejection sampling function  $s(x)$  that is a sum of positive terms. The function is determined by the user, and can be used as long as  $s(x) \geq \text{Beta}_S(x; a, b)$  when  $0 \leq x \leq 1$ .  $\text{Beta}_S$  is used again here because it will be shown later in this section to be more efficient to calculate than the actual beta pdf. The goal is to pick terms that almost equal the  $\text{Beta}_S$ , and that are easy to integrate and invert so that a random sample can be drawn from the inverted CDF of  $s(x)$ . Some examples of functions that have easily inverted CDFs are constants, linears, polynomials, and hyperbolic trigonometric functions (e.g. sinh, cosh). For the cases explored  $s(x)$  was made a piecewise function by using heavyside functions  $H(x; c)$  defined as:

$$H(x; c) = \begin{cases} 0, & x < c \\ 1, & x \geq c \end{cases} \quad (14)$$

where  $c$  is the  $x$  value where the step function goes from 0 to 1. If  $n$  terms were used to make the sampling function, then  $s(x) = s_1(x) + s_2(x) + \dots + s_n(x)$ . Making  $s(x)$  into a piecewise function with the range of each term being  $(x_{i-1}, x_i)$  with heavyside functions would look like:

$$s(x) = \sum_{i=1}^n s_i(x) H(x, x_{i-1}) H(x, x_i) \quad (15)$$

where for a beta distribution  $x_0 = 0$ , and  $x_n = 1$ .

The first set of terms explored was a combination of sinh functions on either side of the  $Beta_S$  peak, and a constant around the peak. The issue was finding a consistent way to calculate the sinh coefficients so it would be as close to  $Beta_S$  as possible. This was especially difficult when either beta parameter was much less than the other, meaning the peak was very close to either one or zero. Another method explored used a system of two or four linears, and a constant. Two linears, one on each side of the peak, and a constant around the peak was implemented first. Each linear went from either zero or one to the inflection point of  $Beta_S$  on its respective side of the peak. The inflection points of  $Beta_S$  were found by setting its second derivative equal to zero and solving for  $x$ . Equation (16) shows this solution and its derivation can be found in Appendix C.

$$x = \frac{a^2 + a(b - 1) \pm \sqrt{ab(a + b - 1)}}{a^2 + (b - 1)b + a(2b - 1)} \quad (16)$$

where  $a = \alpha - 1$ ,  $b = \beta - 1$ , and  $\alpha$  and  $\beta$  are the beta distribution parameters.

Once the inflection points are known, the area under each of the lines and constant was calculated, and then normalized so their sum was equal to one. This gives a probability of selecting each one of the functions. A random number ( $\xi_1$ ) is drawn and determines which of the functions will be sampled. If one of the lines is selected Equation (17) is used to sample from its inverted CDF. The derivation of Equation (17) is shown in Appendix D, and includes some simplifications when either  $s_0 = 0$ , or  $s_1 = 1$ .

$$u = \frac{(s_0 + s_1)\xi_2}{s_0 + \sqrt{s_0^2(1 - \xi_2) + s_1^2\xi_2}} \quad (17)$$

$$x = (1 - u)x_0 + u(x_1)$$

where  $s(x)$  is the linear sampling function,  $x_0$  the lower bound used,  $x_1$  the upper bound used,  $s_0 = s(x_0)$ ,  $s_1 = s(x_1)$ , and  $\zeta_2$  is the second random number drawn.  $u$  is the inverted value of the sampling function CDF with a range of  $[0,1]$ . Once  $u$  is known the value of  $x$  can be calculated. This makes sense because when  $u = 1$ ,  $x = x_1$ , and when  $u = 0$ ,  $x = x_0$ , which are the upper and lower bounds of the sampling function chosen. If the portion of  $s(x)$  randomly chosen is the constant then there is no need to find the inverse of the CDF, it is simply  $u = \zeta_2$ , and  $x$  is calculated from the same equation as the linear. Now that  $x$  has been determined,  $\text{Beta}_S(x; a, b)$  and  $s(x)$  are calculated. A third random number ( $\zeta_3$ ) is drawn and if  $\zeta_3 s(x) \leq \text{Beta}_S(x; a, b)$  then  $x$  is accepted as the random sample, otherwise it is rejected and the process begins again. Shown below is a sample algorithm that generalizes this process with  $n$  piecewise terms.

```

Function Sample_Beta_Linear(alpha, beta, n) Result(SampleX)
  Use Kinds, Only: dp
  Use Random_Numbers
  Implicit None
  Real(dp), Intent(In):: alpha, beta
  Integer, Intent(In):: n !number of linear terms to use
  Real(dp):: SampleX, y, PDF
  Real(dp):: a, b, u
  Real(dp):: x(0:n), s(0:n), Area(0:n), xi(1:3)
  Integer:: i

  a = alpha - 1._dp
  b = beta - 1._dp
  !Find x values where piecewise terms meet
  x(0) = 0._dp
  ForAll (i = 1:n-1) x(i) = Calc_x_Piecewise_Points(i, a, b)
  x(n) = 1._dp
  Area = 0._dp
  Do i = 0, n
    !Find y values where piecewise terms meet
    s(i) = Sampling_Function_Value(i, x(i))
    !Calculate area under line for probability of selecting it to sample from
    If (i > 0) Area(i) = Get_Area_Under_Curve(x(i-1), x(i), s(i-1), s(i))
  End Do
  Area(0) = Sum(Area(1:n))
  ForAll (i = 1:n) Area(i) = Area(i)/Area(0)

```

```

Do
  !Get random numbers
  xi = Random_Vector(3)
  Do i = 1, n
    !Check to see which line to sample from first random number
    If(xi(1) <= Sum(Area(1:i))) Then
      !Calculate u from lines inverse CDF using second random number
      u = Inverse_CDF_line(xi(2), x(i-1), x(i), s(i-1), s(i))
      !Calculate x from u, and y of sampling function from x
      SampleX = (1._dp-u)*x(i-1)+u*x(i)
      y = Sampling_Function_Value(i, SampleX)
      Exit
    End If
  End Do
  !Calculate value of standardized beta PDF from x drawn
  PDF = Beta_PDF(SampleX, a, b)
  !Check for acceptance by comparing PDF value to third random number
  !times the value of the sampling function
  If (xi(3)*y <= PDF) Exit
End Do

```

Using two linears that go from either zero or one to the inflection points and a constant does improve the parsimony of random sampling over having no rejection scheme, however this improvement is diminished greatly as either beta parameter becomes much greater than the other. Figure 6 shows  $Beta_5(x; 50, 450)$  and the sampling functions with three terms as an example of when this happens.

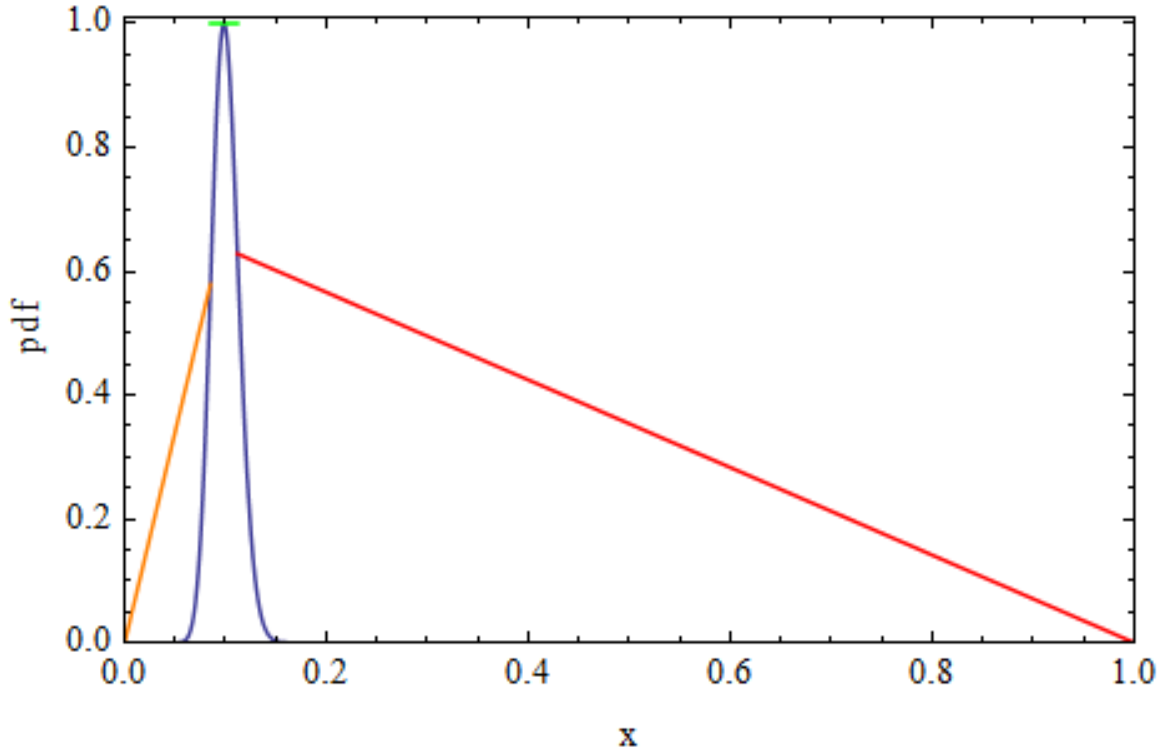


**Figure 6.  $\text{Beta}_s(x; 50, 450)$ , orange and red lines are rejection sampling functions from 0 to the 1<sup>st</sup> inflection point, and 2<sup>nd</sup> inflection point to 1 respectively. Green line represents constant sampling function around the peak of  $\text{Beta}_s$ .**

What is apparent from Figure 6 is that if the areas under the three sampling functions are compared, the area under the red curve dominates. This means the red line will be chosen to sample from a majority of the time. The problem is the value of  $\text{Beta}_s$  under the red line is almost zero making the probability of the third random number being less than the  $\text{Beta}_s$  very small. This highlights the need for another set of lines that start at 0 and 1 and go to points very close to where the peak begins to rise. Consistently being able to find these points over a wide range of beta parameters is the challenge. Equations (18) and (19) were empirically determined and represent these points, the derivation of which is shown in Appendix E. As in development of the beta distribution

inflection point,  $a = \alpha - 1$  and  $b = \beta - 1$ , where  $\alpha$  and  $\beta$  are the beta distribution parameters.

$$x = \frac{a + b + S_R - \sqrt{(a + b + S_R)^2 - 4aS_R}}{2S_R} \quad (18)$$

where  $S_R$  is the relative slope ( $\text{Beta}_S'(x; a, b)/\text{Beta}_S(x; a, b)$ ) to the left and right of the peak are:

$$S_R = \frac{\pm(a + b)}{e^{\log_{10}(a)-1}} \quad (19)$$

Now a system of four lines and one constant can be used. The first line goes from zero to the positive relative slope point in Equation (18). The second line goes from this point to the first inflection point. The constant covers the area between the two inflection points. The third line goes from the second inflection point to the negative relative slope point. The last line covers from the negative relative slope point to one. Figure 7 shows the same  $\text{Beta}_S(x; 50, 450)$  from Figure 6, but with this new set of sampling functions.

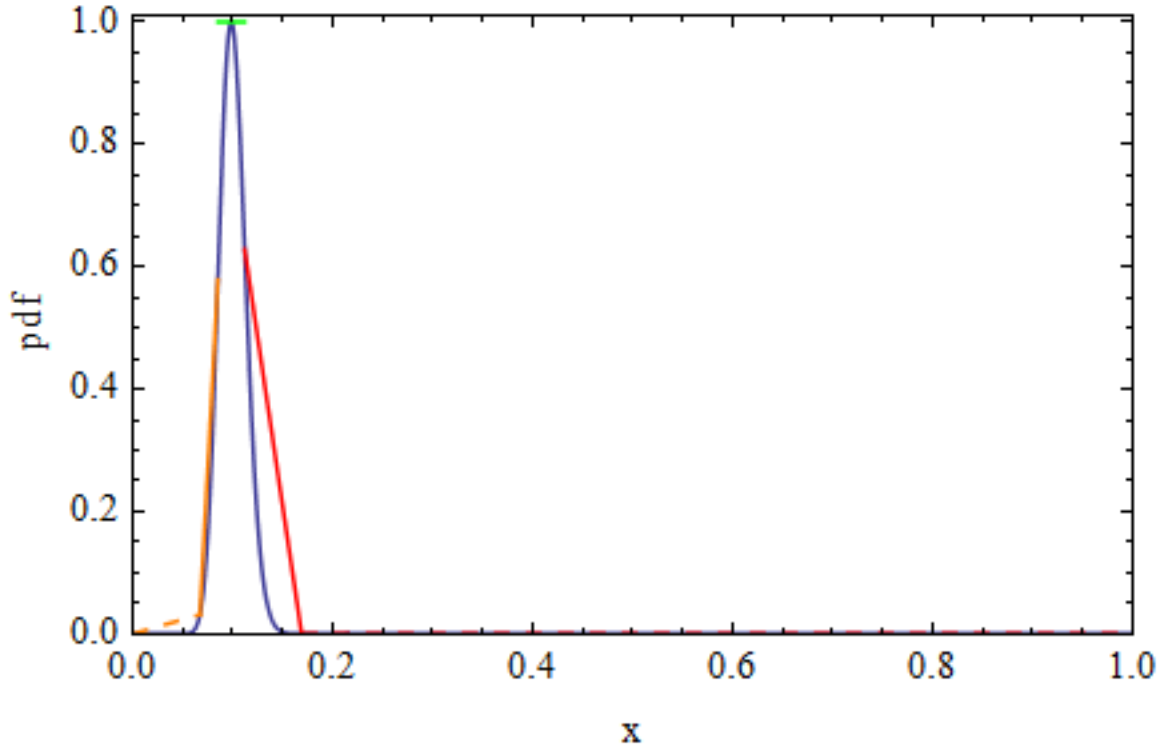


**Figure 7.  $Beta_s(50, 450)$ , orange, and red lines represent the four linear rejection scheme. Green line represents constant sampling function around the peak of  $Beta_s$ .**

The two lines that cover from zero and one to the relative slope points can barely be seen in Figure 7, but neither can  $Beta_s$ . This makes the four linear sampling scheme much more desirable, because the area under the two relative slope curves is very small compared to the constant and other two lines. This means the relative slope lines are selected far less to sample from, and when they are sampled there is a higher probability the sample will be accepted. If efficiency is considered to be the area under the  $Beta_s$  curve compared to the area under  $s(x)$  then Figure 7 is much more efficient than Figure 6. The four linear and constant scheme was tested for a wide range of beta parameters ranging from 1 to  $10^{15}$ . All test cases ended up having acceptance rates from 50% to 75%, with a majority being in the low 60% range.

Now that an effective rejection scheme has been developed, an efficient method for calculating the beta pdf is needed. Recall the equation of the beta pdf with parameters  $\alpha$  and  $\beta$  from Equation (2).

$$\text{Beta}(x; \alpha, \beta) = \frac{x^{\alpha-1}(1-x)^{\beta-1}}{B(\alpha, \beta)}$$

$$\text{where } B(\alpha, \beta) = \int_0^1 t^{\alpha-1}(1-t)^{\beta-1} dt$$

There are two problems with this form of the equation. One, with the integral in the denominator, it makes the calculation computationally expensive due to the need for a table look up or quadrature routine. Two, the distribution peak value varies depending on  $\alpha$  and  $\beta$ . These two issues are solved by standardizing the distribution to where the peak value is equal to one. This is done by dividing Equation (2) by its peak value. This gives a standardized pdf ( $\text{Beta}_S(x; a, b)$ ) whose values have a range of [0,1] and eliminates the  $B(\alpha, \beta)$  integral through cancellation. Doing this along with the simplification of using  $a = \alpha - 1$ , and  $b = \beta - 1$ , yields Equation (20).

$$\text{Beta}_S(x; a = \alpha - 1, b = \beta - 1) = \frac{(a+b)^{a+b}}{a^a b^b} x^a (1-x)^b \quad (20)$$

Equation (20) is now computationally inexpensive to calculate. A new issue arises with the exponent  $(a+b)$  in the numerator. Numerical overflow can now occur, and testing revealed it does using double precision when  $a+b > 143$ . This limit is not acceptable, as  $\alpha$  and  $\beta$  values from Dirichlet distributions for isotopes can be as large as  $10^{12}$ . To solve the overflow issue logarithms are used. Now  $\text{Beta}_S$  can be represented by Equation (21) without concern for numerical overflow.

$$\text{Beta}_S(x; a, b) = e^{(a+b)\log(a+b) - a\log(a) - b\log(b) + a\log(x) + b\log(1-x)} \quad (21)$$



Equation (21) uses five logarithms and one exponential evaluations rather than five and five in Equation (20). Equation (21) is expected to take only 60% as long to compute. This was confirmed in testing over a range of  $\alpha$  and  $\beta$  values that did not overflow Equation (20). A derivation of all three equations can be found in Appendix B. With a well-conditioned and relatively computationally inexpensive method for calculating the value of  $Beta_s$ , all the pieces are in place to draw random samples for branching fractions. This allows for calculation of isotope quantities at later times in an efficient manner.

### III. Implementation

The program is divided up into six main modules: reading in the problem and input data, mapping and organizing the isotope and gamma data, sampling from distributions for half-life and branching fraction uncertainties, building decay chains and generating the transmutation matrix (T-matrix), calculating isotope quantities using the exponential moment functions, and finally calculating statistics and writing the output files. This chapter will lay out details for each of these modules except for decay chain/T-matrix generation, and exponential moments calculations. These modules only have minor changes from Harr's [1] code such as variable name changes and interfaces with other subroutines/modules. A flowchart that includes how all the subroutines and functions interact and are organized into modules can be found in Appendix A.

#### Code Design

The code was written in Fortran 95 using the Microsoft Visual Studio 2010 development suite. Fortran was chosen for its speed in performing mathematical calculations, and simple programming language. Several helper modules/subroutines are included in the code. These include sorting routines, random number generators, timing routines, a variables module, a files module, and a kinds module. The sorting routines and random number generators are self-explanatory. The timing routines calculate the exact time in seconds in linear or log time (specified in the input data), as well as the total number of times to be run. The variables module holds all the global variables of any type used in the code. This makes it easy to find information on any variable that is used in multiple routines, and minimized parameters that need to be passed between routines

and functions. The files module holds an organized list of named integers that represent the external/internal unit specifier for writing and reading files. This is helpful to ensure that the same unit specifier is not inadvertently used in different routines when files are still open. The kinds module has specifiers for single, double, and quadruple machine precision for numbers. Currently the entire program uses double precision and is able to sample from distributions and perform calculations without loss of precision. There may be cases in the future when a small enough branching fraction is measured that would require quadruple precision. Another possible need for greater precision arises if uncertainties in fission fragment yields are sampled.

### **Input Data**

The first information read into the program is the problem data. This file holds the names of the isotope and gamma data files, as well as the initial isotope formation files. It also defines which uncertainties will be used, half-life and/or branching fractions. As a holdover from the Harr [1] code, activity calculations and their outputs is also an option. Other options include linear or logarithmic time steps, and their start and stop time or decades. The value of  $\phi$ , discussed in the Assumptions section is also set in this file. Some other performance options are the number of Monte Carlo trials to perform, the maximum number of decays per chain, and the line number in the isotope data of the highest parent isotope present. The maximum number of decays per chain has to do with array allocation, thus memory use. With the current data being used the longest decay chain is 25 isotopes long. This is a good number to start with, however the option is put in the problem data because as new isotope data is published decays chains can

potentially grow. The highest parent isotope present will have the program only build the T-matrix and do quantity calculations up to this specified isotope. This can dramatically increase the speed of the program, but is dependent on the initial isotopes present. For the different types of neutron induced fission used in this work, the highest isotope initially present was Lutetium 172. As a safety margin the highest parent isotope was input as Francium 233. This increased program efficiency by ~15% over calculating all known isotopes.

The next file read into the program is the isotope data file. This comes from the National Nuclear Data Center's NuDat 2.6 database [2]. The specific format used comes from the Nuclear Wallet Cards output with uncertainties in the Nuclear Data Sheets style. The data is first sorted by number of protons Z, then by number of neutrons N, then by meta stable state or Energy, and lastly by branching fraction percent. All columns are read in, but only the Z, N, Energy, T1/2 (txt), T1/2 (seconds), Dec Mode (decay mode), and Branching (%) columns are used by the program. A sample of the data format is shown in Table 1, and skips from isotope H6 to Na24 to show a metastable state via the Energy column.

**Table 1. Sample Nuclear Wallet Card output from the NuDat 2.6 database.**

A	Element	Z	N	Energy	Mass Exc	Unc	T1/2 (txt)	T1/2 (seconds)	Abund.	Unc	Dec Mode	Branching (%)
1	N	0	1	0	8.0713	5	10.183 M 17	610.98	-1.00E+03	-1000	B-	100
1	H	1	0	0	7.2889	10	-1000 STABLE NA	-1000	1.00E+00	70	X	-1000
2	H	1	1	0	13.136	15	-1000 STABLE NA	-1000	1.15E-04	70	X	-1000
3	H	1	2	0	14.9498	22	12.32 Y 2	388800000	-1.00E+03	-1000	B-	100
5	H	1	4	0	32.89	9	5.7 MEV 21	7.995E-23	-1.00E+03	-1000	2N	100
6	H	1	5	0	41.9	3	1.6 MEV 4	2.848E-22	-1.00E+03	-1000	N	100
24	Na	11	13	0	-8.4179	4	14.997 H 12	53989.2	-1.00E+03	-1000	B-	100
24	Na	11	13	0.4722	-7.9457	4	20.18 MS 10	0.0202	-1.00E+03	-1000	IT	99.95
24	Na	11	13	0.4722	-7.9457	4	20.18 MS 10	0.0202	-1.00E+03	-1000	B-	0.05
25	Na	11	14	0	-9.3578	12	59.1 S 6	59.1	-1.00E+03	-1000	B-	100

The next file(s) to be read in is the initial isotope quantity data. These files contain the Element, A number, metastable state, and initial quantity. A sample of the format is shown in Table 2. Multiple files with different initial quantity information can be used. As will be seen later in the Output Statistics and Data section the different initial amounts will have their own rows or columns in all the different output files.

**Table 2. Sample format for the initial isotope quantity input.**

A	Element	Meta	Amount
67	Mn	0	1.58E-09
67	Ni	0	1.17E-06
67	Zn	0	1.92E-10
68	Co	0	2.23E-06
68	Cu	1	3.76E-07
68	Cu	0	1.39E-07
68	Fe	0	1.61E-07

The initial isotope quantities used for this study were eight types of neutron induced fission. They were U235 fission with thermal, fast, and high energy neutrons;

U238 fast, and high; as well as Pu239 thermal, fast, and high energy neutrons. The data used for these different fissions comes from England and Rider [5]. Neutron induced fission was chosen because it realistically yields the largest number of initial isotopes (average of 821). This brings into play as many decay chains, and initial quantities at different points in the chains as possible.

Once the initial quantities have been read in, the isotopes of interest file is read in to the program. This file lists all the isotopes for which output files will be written. This could be from one to all known isotopes. The reason for this file is if all isotopes are output it will take more time to write all the output files, and will most likely take up in the gigabyte range of hard drive space. If the user is interested in all isotopes, a separate program was written that can read in the same isotope data file and output an isotope of interest file that includes all isotopes. It is recommended that if the isotope data file is modified or a new one is created, to run it through this other program to ensure all potential isotopes are included.

The last files to be read are those needed if activity is going to be calculated. These files for gamma data, and gamma bin information are in the format used by Harr [1]. As a final note for this section, all the input files except for the problem data file require an extra header line that gives either the total number of lines in the file, or number of isotopes of interest, number of initial quantity files, etc. After any changes to a file this number needs to be checked before the program is run.

## Isotope Data

Once all the input data has been read in, some checking, manipulation, and mapping of the isotope data needs to be done. The first is a branching check of all isotopes. Before a check is done to make sure each isotope's different decays add up to one, some things are changed. For instance in cases where an isotope undergoes B- decay and something else at the same time the NuDat data includes that other portion of the decay in the B- branching fraction. As an example let's say an isotope undergoes just B- decay 95% of the time, and B- plus alpha decay 5% of the time. The NuDat data will show two lines one with B- as 100, and BA (for B- plus alpha) as 5, the fractions of which do not sum to one. The branching fraction check subroutine corrects issues like these by simply looking for the subsets of B- and electron capture decay and subtracting them accordingly. After this is done the decay fractions of each isotope is summed and if it is not within a set tolerance of one, the line number, Z, N and branching fraction sum of the isotope is written to an error file.

After the branching fraction check, if half-life uncertainty is used a subroutine will take the text portion of the isotope data input file and extract the standard deviation and turn it into a real number. There are cases where the standard deviation is quoted as different numbers above and below the mean. In this case it will calculate two standard deviations, one that is used for values above the mean and one for below the mean.

The last thing done to the isotope data is to map each decay to its daughter isotope. This is done by going through each decay from the isotope input data file and selecting the case it matches. That case will determine how many protons, neutrons, or metastable states to add or subtract from the parent isotope. It will then find where this

daughter isotope is within the isotopes array and put a pointer for that decay to it. If a case for the decay is not found it is written to an error output file. Currently a majority of the decay type errors are spontaneous fission. The program does not currently deal with spontaneous fission. This is not an issue because all of the initial isotopes formed for this study and their daughters do not have enough protons and neutrons to fission spontaneously.

Once these routines are done with the isotope data, similar routines go through the gamma data per Harr [1]. Once this is done, initialization of the program is complete. The first Monte Carlo trial is started and uncertainties are sampled from their respective distributions.

### **Distribution Sampling**

If half-life uncertainty is a selected option, then a sample for each isotope is drawn from a normal distribution. This is done by drawing 12 random numbers, summing them and subtracting 6. If the isotope has two standard deviations, the one for below the mean is used if the value is negative, and the one for above the mean is used if the value is positive. The value is then multiplied by the standard deviation and then added to the mean to get the random sample.

$$t_{HL} = \mu_{HL} + \sigma_{HL} \left( \sum_{i=1}^n \xi_i - \frac{n}{2} \right) \quad (22)$$

where  $t_{HL}$  is the randomly sampled half-life,  $\mu_{HL}$  and  $\sigma_{HL}$  are the half-life mean and standard deviation respectively,  $\xi$  is a random number in (0, 1), and  $n$  is the number of random numbers drawn (12 in this case). This method is not very parsimonious with



random numbers, but is efficient computationally and covers +/- six standard deviations from the mean. It was also done because as Harr [1] discovered by contacting the National Institute of Standards and Technology (NIST), isotopes with these two standard deviations represented normal distributions with different standard deviations on each side of the peak.

If branching fraction uncertainty is selected then the method laid out in the Sampling Beta and Dirichlet Distributions section is used. This method is not as straightforward as the half-life uncertainty sampling method. First, each isotope is checked to see if it has multiple branches. If there are multiple branches then a Dirichlet sampling routine is called with the isotope information and number of branches. Based on the means of each branch and the input parameter  $\phi$ , the sum of the concentration parameters is calculated and then each concentration parameter individually. From there a subroutine that implements the rejection scheme developed earlier is called to get a random sample for each branching fraction. After all branches of an isotope are randomly sampled, they are normalized so their sum is equal to one. This process is then repeated for all isotopes.

### **Output Statistics and Data**

The last piece of the program takes all the quantity calculations and performs some statistical calculations and outputs the data to text files for analysis. After each Monte Carlo trial a routine is called that writes the quantity values for each isotope of interest to a file. When complete there is a separate file for each isotope of interest that contains all times run, all initial quantity inputs, and the quantity values. If there are

numerous isotopes of interest, writing all the quantity values to a file will take up a large amount of memory, as well as time. In the cases run for this study that did 1,000 Monte Carlo trials, with 31 different times, and 8 initial quantity inputs each isotope had a file size of approximately 4.5 Megabytes. With all known isotopes input as isotopes of interest it takes up about 3.6 Gigabytes of disk space for each run. If an isotope of interest has quantity values of zero at all times run, for all initial quantity inputs then a file will not be created for it. This is done as to not waste disk space, and computer time writing out zeros to a file. Because of the potential need for large amounts of disk space, writing out all these quantity values is an option that is specified in the problem data file.

Once all the Monte Carlo trials are completed, the mean and standard deviation of each isotope of interest is calculated from its quantity values. If the isotope of interest has values greater than zero at any time run then two files are opened one for its mean and the other for standard deviation. Its respective mean and standard deviations are then written to these files for each time and initial quantity input.

Another option in the problem data is to output the overall statistical data. If this option is marked true then the relative standard deviation of each isotope of interest present is calculated. Then the average and standard deviation of these relative standard deviations are calculated for each time run and initial quantity input. The results are written to two files. A third file is written containing a list of the relative standard deviations with isotopes from greatest to least for each time and initial quantity. This allows the user to see which isotopes of interest have the largest relative standard deviations.

## Verification

To ensure the overall code performed as expected the modules themselves and even routines/functions were tested individually. More in depth verification was done specifically for beta distribution sampling. A Monte Carlo program was written that would randomly sample a beta distribution with and without rejection schemes. Test cases had distribution parameters that ranged from 1 to  $10^{24}$ , with any run that had parameters greater than  $10^{15}$  using quadruple precision. Because random samples were being taken the outputs were not exact. For test cases performed with 1,000 Monte Carlo trials the mean and standard deviation only varied by one hundredth of a percent.

Beta pdf values were verified by using the same range of parameters above and comparing results from Equation (21) to results from Equation (20). This proved that Equation (21) would not overflow while returning an answer that had the same precision as Equation (20) to 13 digits.

The overall isotope quantity outputs were verified by comparing the output of the program without half-life or branching fraction uncertainty to a separate program that calculated these same quantities using both a numerical integration solution and a Bateman equation solution. The outputs between the Bateman solution and the program (exponential moments solution) typically had maximum relative errors of around  $10^{-8}$ . The relative error between the numerical integration solution and the program had maximums of  $10^{-2}$ .

## Performance

All runs and development were done on a Dell XPS 8300 with an Intel i7-2600 processor at 3.40 GHz, and 12 gigabytes of RAM. The operating system is Windows 7 Professional 64 bit, Service Pack 1. The development suite used was Microsoft Visual Studio 2010 version 10.0.30319.1, with the Intel Visual Fortran Composer XE 2011 Update 9, version 12.1.3526.2010. The program can be compiled to run using either 32 or 64 bit. Initially Intel's auto parallelization mode was selected when compiling but after testing it was found disabling it actually decreased run times by about 75%.

Typical run times using this setup along with 1,000 Monte Carlo trials, 31 time steps, all known isotopes as isotopes of interest, and 8 different initial quantity inputs were around 2.5 hours. The run time is most sensitive to the number of Monte Carlo trials and the number of time values. Program initialization takes about 45 seconds, and writing final statistics to files takes only a few seconds. Each Monte Carlo trial has an overhead computation time of about one second, which is primarily the time needed to sample all the half-life and branching fraction uncertainties. This means each time step, or the time it takes it to generate a transmutation matrix and calculate all the exponential moments, takes about 1/4 of a second.

The same setup uses approximately 150 megabytes of RAM while running. This relatively low memory requirement is achieved by writing out the individual isotope quantity amounts after each Monte Carlo run. If this was not done the same run would require almost 5 gigabytes of RAM during a run. This is an issue for two reasons. One 32 bit Windows systems cannot handle arrays that require more than 2 gigabytes of

memory. Two it places a large strain on a majority of PCs currently in use, and eliminates the possibility of doing two runs on the same computer at once.

As mentioned earlier the time to sample all the branching fractions and half-lives currently takes about one second, which is about 11% of the computer time. This is with the sampling rejection scheme that uses four linears and a constant. If no rejection scheme is implemented the number of random numbers used explodes and the sampling routine dominates the program runtime. To test the rejection scheme's performance a program run with the same inputs as one of the analysis runs was done. Counters were added to record the number of calls to the beta pdf sampling routine as well as the number of random numbers used. For one Monte Carlo trial without a rejection scheme the beta pdf was called 2,179 times, and used 5,997,231,659 random numbers. That is an average of 2,752,286 random numbers per call to the routine. The run took 53 minutes, which is over a 3,000 times increase in run time. With the rejection scheme the sampling routine was called the same number of times (2,179), but used only 10,464 random numbers. That is an average of 4.8 random numbers for each call to the routine. The minimum number of random numbers the routine uses is three, which means it has an average acceptance rate of 63%. This proves the need for and effectiveness of the four linear and constant rejection scheme over a wide range of beta distribution parameters.

Program run times are on the order of 1 to 3 hours for 1,000 Monte Carlo trials. Further improvements could be found in how the transmutation matrices are generated. The next step that would most likely yield the most improvement in run time is to save all the decay chains to an array, so it only has to be calculated once.

#### IV. Results and Analysis

To investigate the effect of branching fraction uncertainty on isotope quantities, four branching fraction relative standard deviation percentages (defined as  $\phi$  in the Sampling Beta and Dirichlet Distributions section) were explored: 1%, 5%, 10%, and 20%. For each of these  $\phi$ s, two separate runs were completed, one where only branching fraction uncertainties were used, and another where both branching fraction uncertainties and half-life uncertainties were considered. A single run was done with only half-life uncertainties, because it is independent of  $\phi$ . Short hand notation is used hereafter for each type of run done, BF for branching fraction uncertainty only, HL for half-life uncertainty only, and HLBF for runs done with both these uncertainties.

The fission fragment yields from three neutron spectrums of three different isotopes were used as initial quantity values. The neutron spectrums were thermal, fast (fission energy neutrons), and high (fusion energy neutrons). The three fuel isotopes were U235, U238, and Pu239 (note: U238 does not have a thermal fission cross section, so no data for this case is presented). This makes eight initial quantity values that will henceforth be referred to by their fuel isotope then neutron spectrum (e.g. Pu239 high or U235 thermal).

The time values were logarithmic starting at  $10^{-1}$  seconds and ending at  $10^9$  seconds (~31.7 years), with three time values per decade. The range was chosen because it represents times of interest for nuclear forensics and fallout prediction, and was a large enough range to recognize and analyze trends. 1,000 Monte Carlo trials were performed for two runs with the same input parameters to compare relative error. This was done to

see if 1,000 Monte Carlo trials was a statistically large enough sample. Between the two runs, the mean isotope quantities had an average relative error of around  $10^{-4}$ . The standard deviation average relative error was  $10^{-2}$ . This shows the means typically agreed to four digits, and the standard deviations to two digits. Two longer runs with 10,000 Monte Carlo trials were performed and again for the mean the average relative error was  $10^{-4}$ . The standard deviation relative error was  $10^{-2}$ . Because increasing the number of trials to 10,000 had no or very little effect on relative error, 1,000 trials was used for the remaining runs.

### **Uncertainty Ratios**

In order to compare and analyze the quantity of all isotopes present, a metric that is independent of magnitude is needed. This is because the amount of an isotope can vary by orders of magnitude over a period of time, but also the range of quantities between isotopes varies by orders of magnitude. Relative standard deviation ( $\sigma/\mu$ ) is properly suited for this, but in this case its overall statistics get skewed to larger numbers from those isotopes that are rapidly decaying away to zero quantity. When this happens to an isotope its relative standard deviation gets very large, potentially greater than one.

Because of the relative standard deviation problem, ratios of the different standard deviations were used. For each isotope present at a given time the ratio of its standard deviation from the BF run was divided by the standard deviation from the HLBF run ( $\sigma_{BF}/\sigma_{HLBF}$ ). Similarly the standard deviation from the HL run was divided by the standard deviation of the HLBF run ( $\sigma_{HL}/\sigma_{HLBF}$ ). This gives the fraction of uncertainty in an isotope's quantity due to branching fractions and half-lives respectively. The ratios

will be in [0,1], because total uncertainty must increase or remain the same when additional source of uncertainty is introduced. It also avoids the relative standard deviation problem because the mean is not used. If the statement above about the two ratios was accurate then  $\frac{\sigma_{BF}}{\sigma_{HLBF}} = 1 - \frac{\sigma_{HL}}{\sigma_{HLBF}}$ , which is not the case. These uncertainties are not additive because if you change one it affects the other. It was also considered that the sum of the variances from the HL and BF run would equal the variance of the HLBF run, which is not the case either. What is known is that the actual uncertainty due to branching fractions must be between  $\frac{\sigma_{BF}}{\sigma_{HLBF}}$  and  $1 - \frac{\sigma_{HL}}{\sigma_{HLBF}}$ .

To present the results clearly, a count of the number of isotopes whose ratio is greater than a set amount was done. As an example, if the amount was 0.5, then

$$1 - \frac{\sigma_{HL}}{\sigma_{HLBF}} \geq 0.5 \quad \text{or} \quad \frac{\sigma_{BF}}{\sigma_{HLBF}} \geq 0.5 \quad \text{must be true for an isotope to be counted.}$$

The amount 0.5 would count all isotopes that have uncertainty due to branching fractions as the dominant factor. If the amount was 0.2 then all isotopes who have at least 20% of their uncertainty due branching fractions is counted. This count of isotopes is done for both ratios  $\frac{\sigma_{BF}}{\sigma_{HLBF}}$  and  $1 - \frac{\sigma_{HL}}{\sigma_{HLBF}}$  separately, and divided by the total number of isotopes present at that time. This gives a percentage of isotopes that meet the criteria. As mentioned in the previous paragraph the actual number is somewhere between the two ratios. To take this into account the two counts are averaged and error bars show the range between them, Figure 8 shows this for U238 high where uncertainty due to branching fractions dominate.



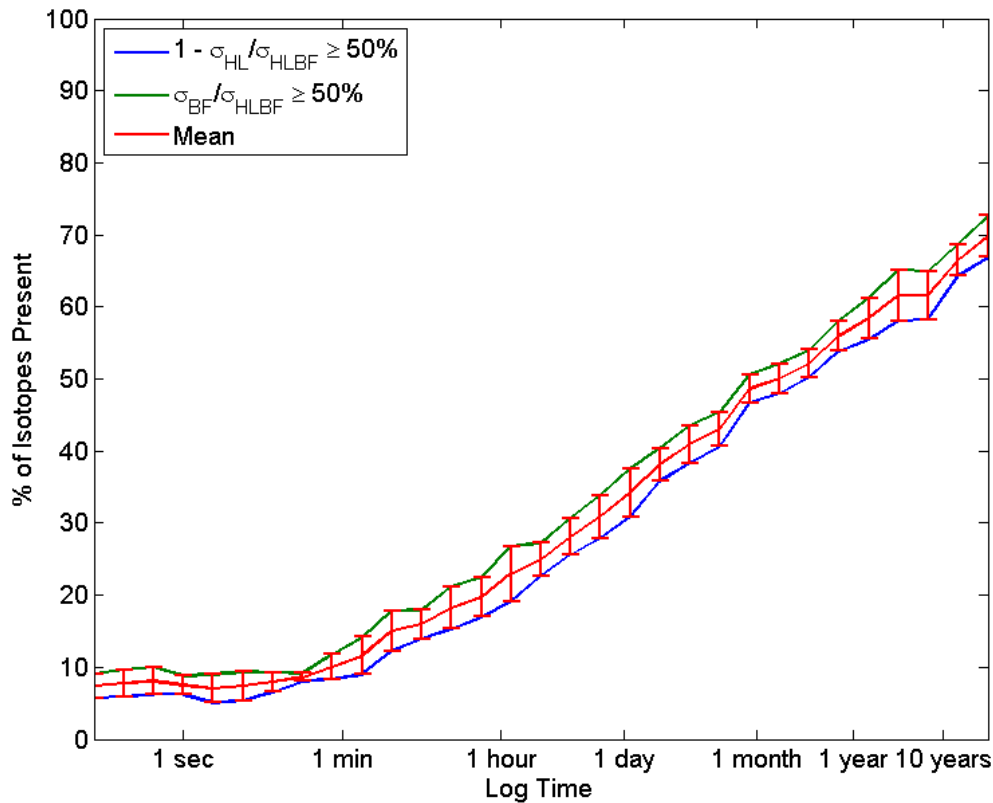
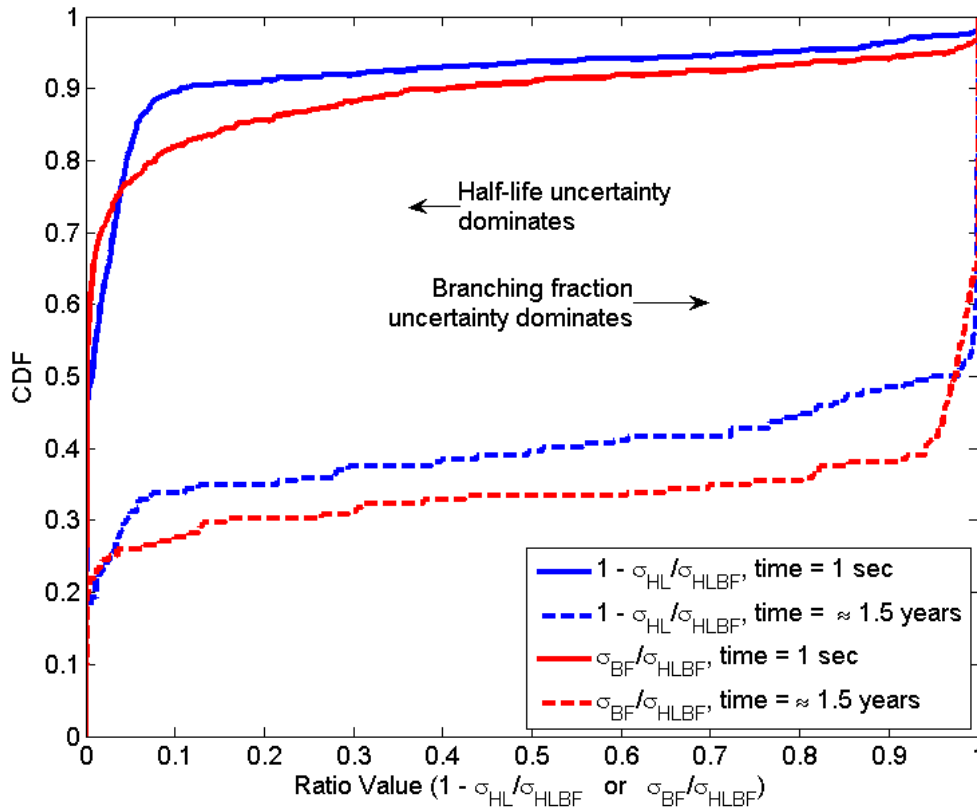


Figure 8. Comparison of uncertainty due to branching fractions ratios as a percent of all isotopes present for U238 high and  $\phi = 10\%$ .

Figure 8 shows that as far as the number of isotopes goes, the difference between the two ratios is typically within 5% of each other. For the other types of fission the shape and magnitude of the curves are similar ( $\pm 2\%$ ). The one with the largest difference is U238 fast, whose percent of isotopes present values are all approximately 5% greater at all times shown.

Figure 8 shows the point at which either uncertainty from half-lives or branching fractions dominate. To get a better idea of what the distribution of these ratios is like an empirical CDF was done at an early time and late time and is shown in Figure 9.



**Figure 9. Comparison of empirical CDFs for the different ratios at 1 second and ~1.5 years for U238 high and  $\phi = 10\%$ . At both times the ratio for most isotopes is either very close to zero or one. This means very few isotopes have uncertainties from both half-lives and branching fractions that are of the same order of magnitude.**

The empirical CDFs in Figure 9 show that at both early and late times the isotopes present either are significantly dominated by uncertainty from half-lives or uncertainty from branching fractions. In all four curves the ratio values go from less than 0.1 to greater than 0.9 in less than 0.2 on the CDF axis. This means less than 20% of the isotopes present at both times have comparable uncertainties from both half-lives and branching fractions.

Another way of showing what is going on and confirms this trend over all times is to graph multiple curves with different ratio values, this is done in Figure 10.

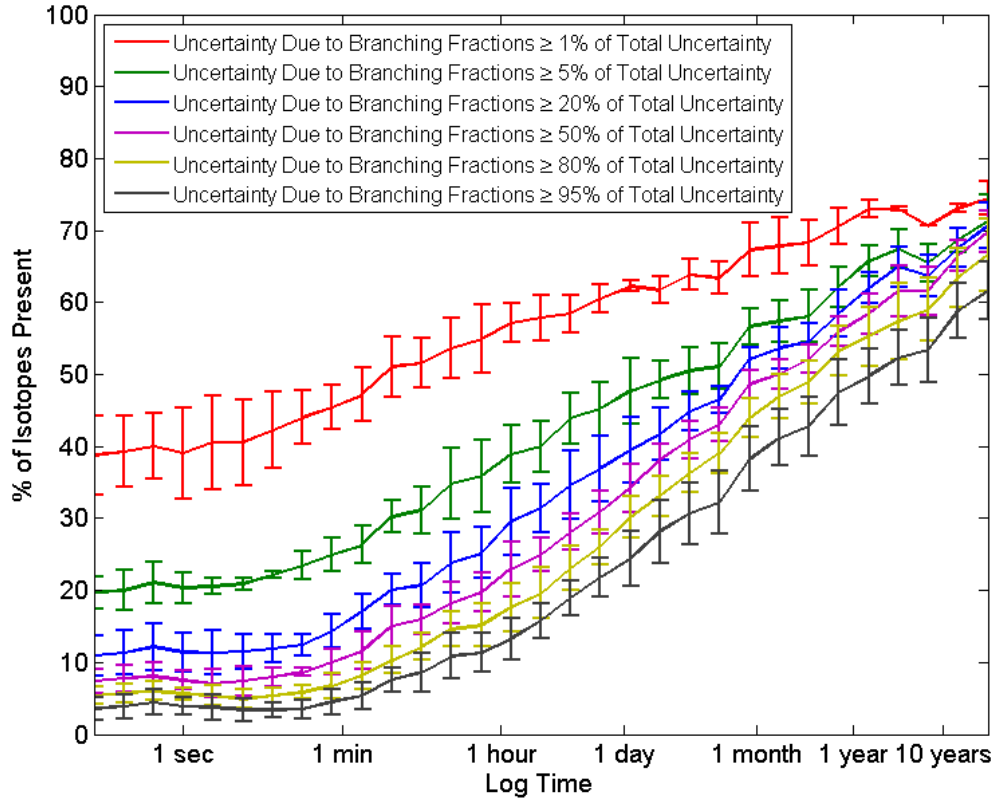


**Figure 10. Comparison of multiple uncertainty ratio values as a percent of all isotopes present for U238 high and  $\phi = 10\%$ .**

Figure 10 shows how closely spaced the ratio values are, meaning at all times a majority of the distribution is either very close to zero or one. Again this supports that for most isotopes their uncertainty is either dominated by half-lives or branching fractions, very few have comparable contributions from both. Both Figure 9 and Figure 10 look at only U238 high with  $\phi = 10\%$ . Other fission types and  $\phi$ s were plotted and showed very similar results.

## Branching Fraction Uncertainty ( $\phi$ ) Results

Now that a method for comparing all the isotopes present at a given time has been developed, the branching fraction uncertainty ( $\phi$ ) can be varied and analyzed. As stated earlier runs were done with  $\phi = 1\%$ ,  $5\%$ ,  $10\%$ , and  $20\%$ . Ratio values of 0.5 were chosen for the curves because it shows the point where either uncertainty due to branching fractions or half-lives dominate the overall uncertainty. Figure 11 shows the effect of varying  $\phi$ .

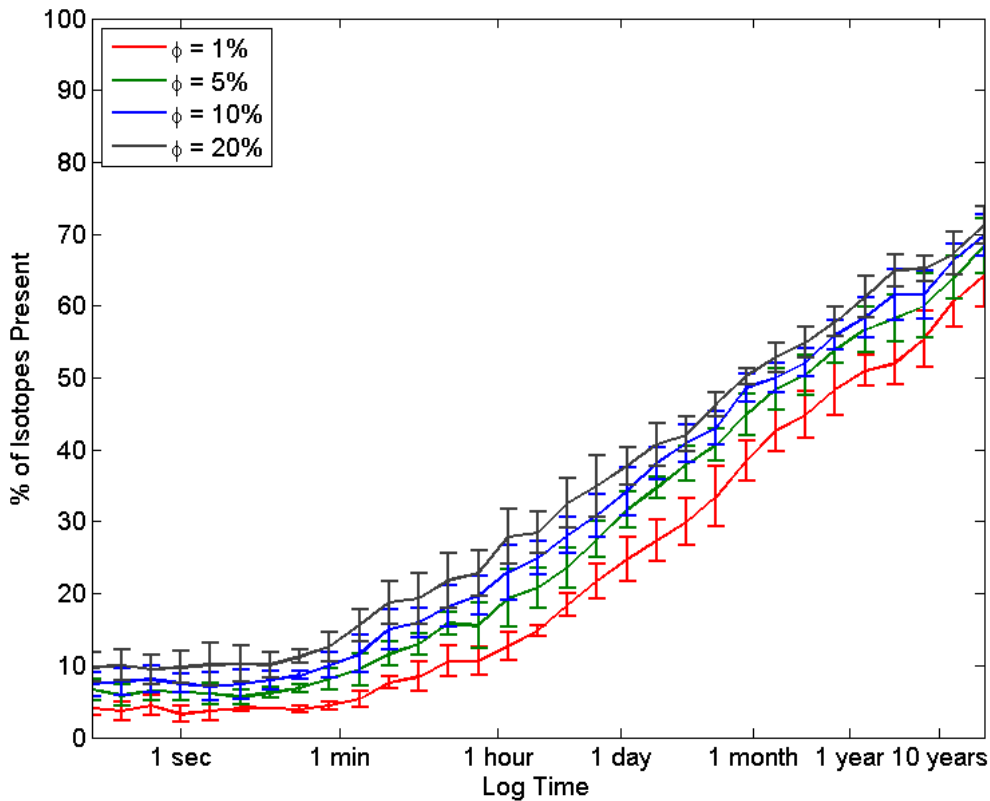
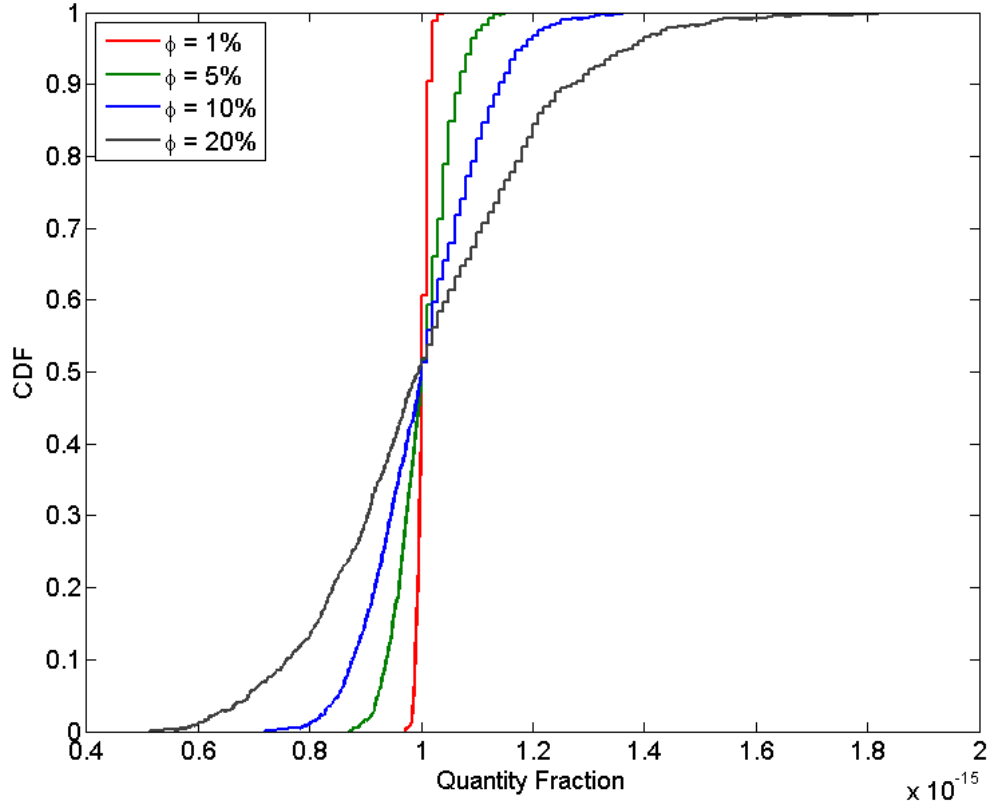


Figure 11. Comparison of Branching Fraction Uncertainties ( $\phi$ ) with ratio values of 0.5 as a percent of all isotopes present for U238 high.

What is apparent in Figure 11 is that changing  $\phi$  has little effect on changing the percent of isotopes it dominates at a given time. Going from  $\phi = 1\%$  to  $\phi = 20\%$  typically only increases the percent of isotopes present by about 10%. It should be noted that at early times the number of isotopes present is around 800, where at late times it dwindles down to a little over 200. The real driving factor is time. There is an increase from less than 10% at less than one minute to around 50% of isotopes present in the month timeframe. The fact that time is a factor makes sense. As isotopes decay away and become very long lived or stable, half-life uncertainty should begin to decrease. This is because half-life uncertainty is only a factor in determining when an isotope will be present. Branching fraction uncertainty is a factor in determining what isotope will be present. So as time passes and more long lived or stable isotopes are present the effect of half-life uncertainty decreases, whereas as time passes and more opportunities for isotopes to branch occur branching fraction uncertainty should increase. What was surprising in Figure 11 is how quickly the curves rise to where a majority of the isotopes present are dominated by branching fraction uncertainty.

As shown in Figure 9 from the previous section the ratio distributions go from zero to one so quickly. This means changing the ratio value in Figure 11 anywhere between 0.05 and 0.95 would raise or lower the curves by only a few percent. This also helps explain as to why there is little difference when  $\phi$  is changed. Because most isotopes are either significantly dominated by half-life or branching fraction uncertainty changing  $\phi$  would have little effect. The driving factor is not how big  $\phi$  is, but the fact that it is present. This applies when analyzing all possible isotopes present at a given

time. If individual isotopes are analyzed varying  $\phi$  can play a role in the magnitude of the uncertainty. The ground state of Sn129 is shown as an example in Figure 12.



**Figure 12. Empirical CDFs of the Ground State of Sn129 with different values of  $\phi$  from U235 thermal at 10,000 seconds.**

As  $\phi$  increases the empirical CDF's range increases, showing that the uncertainty goes up, while the mean remains constant. The standard deviation of these distributions is shown in Table 3, and shows that as  $\phi$  increases the standard deviation increases proportionally.

**Table 3. Quantity standard deviation of Sn129 ground state for varying  $\phi$  at 10,000 seconds from U235 thermal fission.**

$\phi$	1%	5%	10%	20%
Standard Deviation	1.0192e-17	5.0594e-17	1.0319e-16	2.0316e-16

Increasing  $\phi$  does have an effect. However, for most isotopes increasing  $\phi$  as compared to the contribution of uncertainty from half-lives has little effect. This is because the uncertainty from half-lives is most likely either much greater than or much less than the uncertainty from branching fractions.

### Limiting Quantity Fraction

Double precision in Fortran allows numbers to get as small as  $10^{-308}$ . However, this is much smaller than what is needed to realistically track quantity fractions of isotopes. If there are approximately  $1.45e^{23}$  fissions per kiloton of yield Bridgman [6], and the largest potential weapon would be around 100 megatons, this means a quantity fraction would have to be greater than  $6.9e^{-29}$  to be present. For a 1 kiloton weapon this number would be  $6.9e^{-24}$ . Potential collection samples would have to be much larger than this. This number is called the limiting quantity fraction or quantity which we care about or can measure. It is then used as a cutoff where any quantity fraction less than this limiting quantity fraction is not counted in statistics. The limiting quantity fraction can be varied to see how it affects the percentage of isotopes present that are dominated by branching fraction uncertainties.

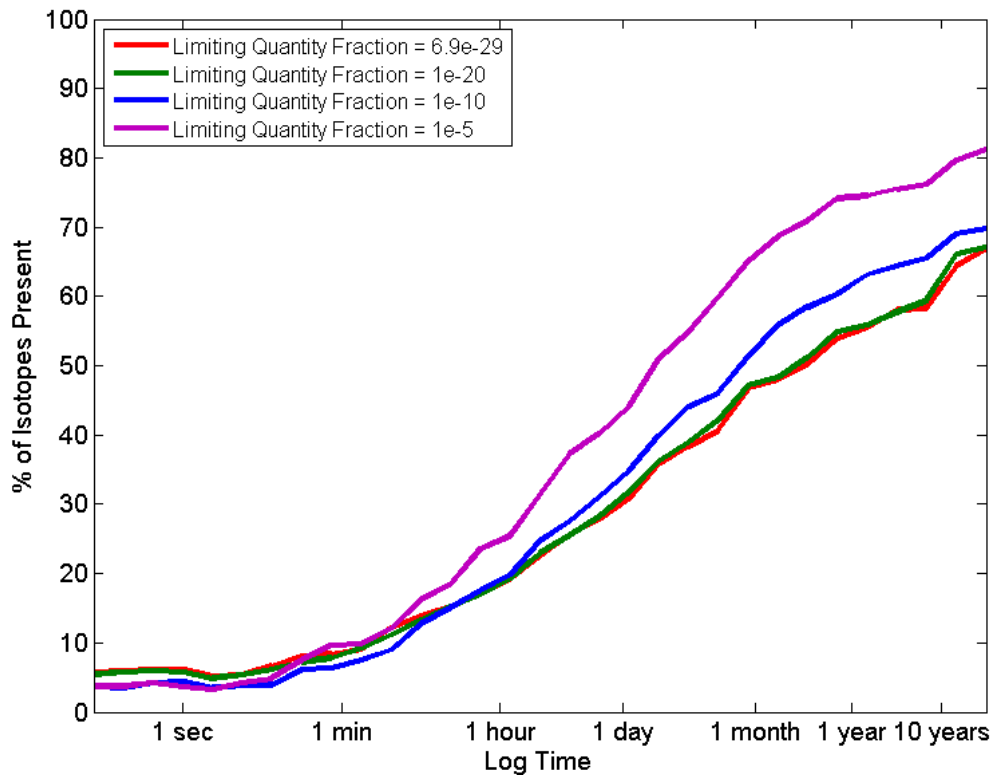


**Figure 13. Limiting quantity fraction effect on percent of isotopes dominated by branching fraction uncertainty for U238 high fission and  $\phi = 10\%$ .**

Figure 13 shows four different minimum quantities showing the line for percent of isotopes dominated by branching fraction uncertainty. The error bars are omitted in this figure so the reader can discern the small differences in the curves. At early times there is very little difference in the curves and all are well within each other's error bars. At late times the smallest two levels are still right on top of each other. This shows there is a level where limiting quantity fraction has little or no effect. The quantity fraction is so small that most isotopes that are at this level are most likely rapidly decaying away to zero. The interesting thing is as the limiting quantity fraction is increased the curves grow in magnitude as time increases. The purple curve representing a limiting quantity



fraction of  $10^{-5}$  is about the top 50% isotopes in quantity. Meaning at early times it only shows about 400 isotopes, and at late times a little over 100 isotopes. This suggests that isotopes present in larger amounts are more likely to be dominated by branching fraction uncertainties rather than half-life uncertainties at later times.

### **Quantity Fraction Distributions**

One of the program outputs is each isotope's quantity fraction mean and standard deviation for each time and initial quantity value. This allows for comparison of isotopes across times or different initial quantities with error bars that represent the standard deviation. In the absence of any additional information, it is common practice to assume that these statistics are normally distributed. The goal of this section is to show when a normal distribution is and is not a good approximation of an isotope's quantity fraction.

Analysis of all isotopes present after fission for all times would be overwhelming. Instead individual isotopes that displayed a particular characteristic across multiple fission types or timeframes were analyzed. This was done to help try and identify trends or attributes. The first isotope chosen was the ground state of Sn129. It was chosen because it is dominated by half-life uncertainty at 10,000 seconds. Figure 14 shows empirical CDFs for a runs with branching fraction uncertainty only, half-life uncertainty only, and with both a branching fraction and half-life uncertainty. Overlaid with dashed lines are normal CDFs with means and standard deviations that match the isotope data.

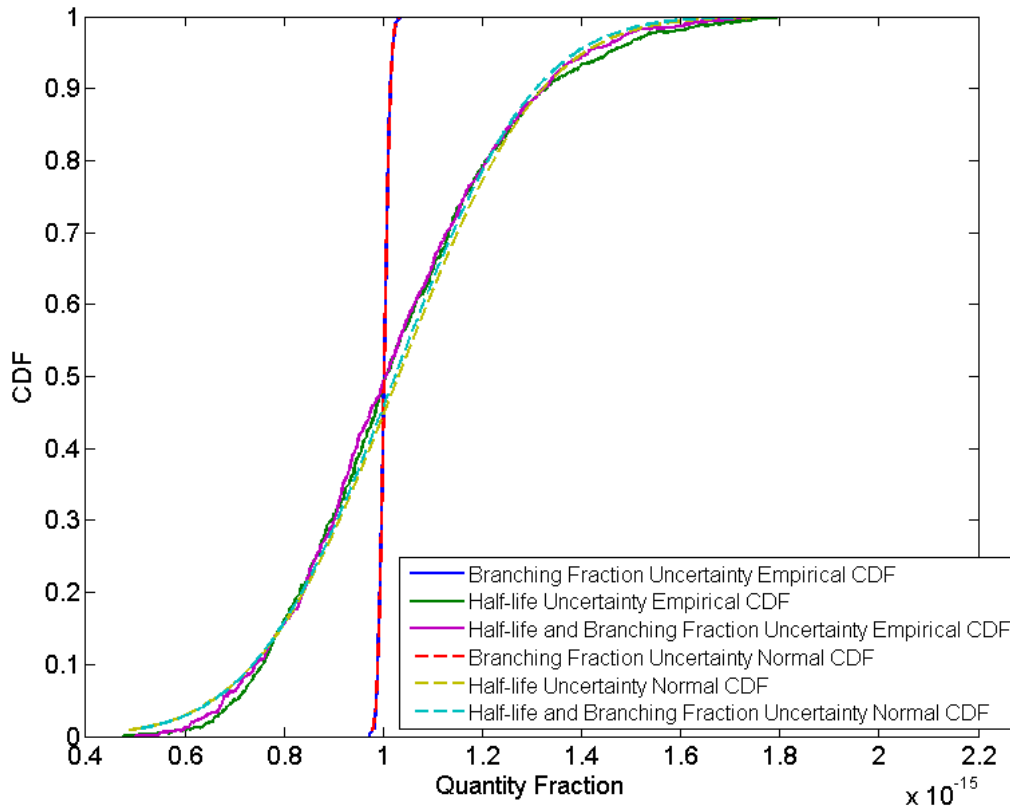


**Figure 14. Empirical CDFs of the Ground State of Sn129 from U235 thermal at 10,000 seconds with  $\phi = 1\%$ , as compared to a Normal CDFs with the same mean and standard deviation.**

As can be seen in Figure 14 when half-life uncertainty is considered compared to branching fraction uncertainty it increases the standard deviation. It also deviates more from a normal distribution in both the tails and around the peak. This carries through to the run when both uncertainties are considered. Even so, all three runs match up closely with their respective normal distributions. The last thing to note about this isotope is it just starting to decay away to zero, and within one more decade or 100,000 seconds it will be gone.

Now an isotope whose uncertainty is dominated by branching fractions will be examined. Te124 is very long lived and is dominated by branching fraction uncertainty for the entire timeframe examined. Figure 15 looks at the distributions at early time 0.1 seconds for all three types of runs.

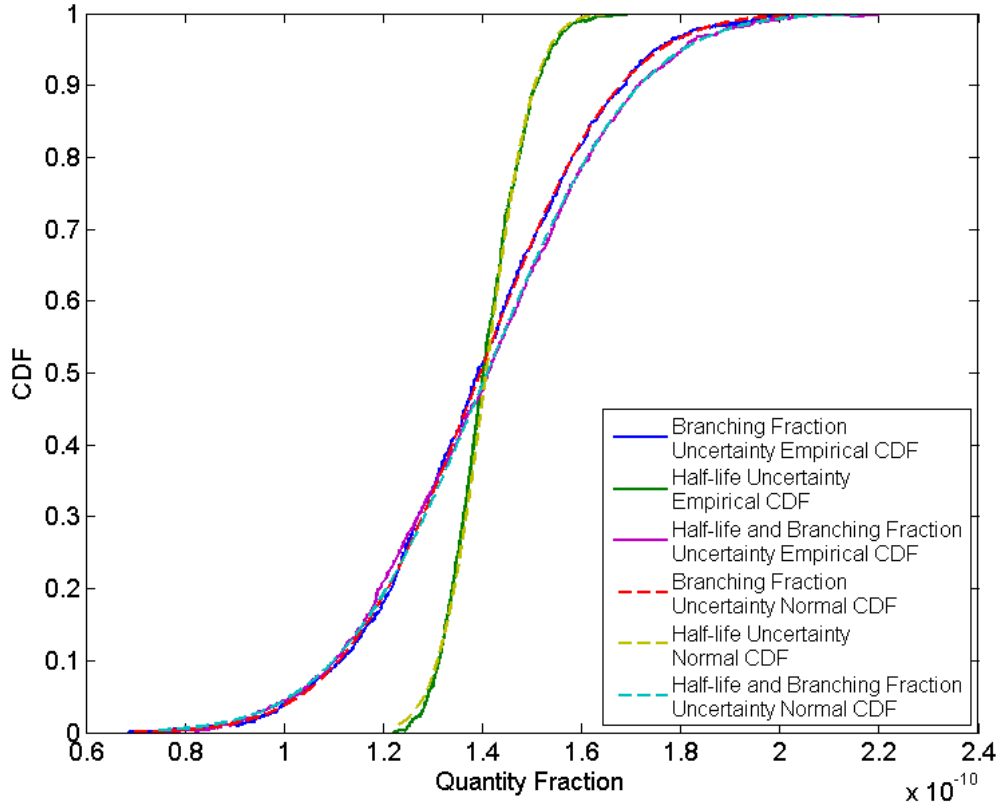


**Figure 15. Empirical CDFs of Te124 from Pu239 fast at 0.1 seconds with  $\phi = 20\%$ , as compared to a Normal CDFs with the same mean and standard deviation.**

Even though branching fraction uncertainty is the dominant factor at this time, the distributions remain very close to normal in Figure 15. Another difference between Figure 14 and Figure 15 is the difference in  $\phi$ . In Figure 14  $\phi = 1\%$ , and in Figure 15  $\phi = 20\%$ , however both curves with branching fraction uncertainty only, match up closely

with their normal. This shows  $\varphi$  does not affect the shape of the distribution. There was some thought that since branching fractions are sampled from beta distributions when the uncertainty gets large it could deviate more from normal distributions than half-life uncertainty, but this looks like it is not the case. During early time Te124 is going through a transient and is increasing in quantity as seen in Figure 16 with a log log quantity versus time plot.

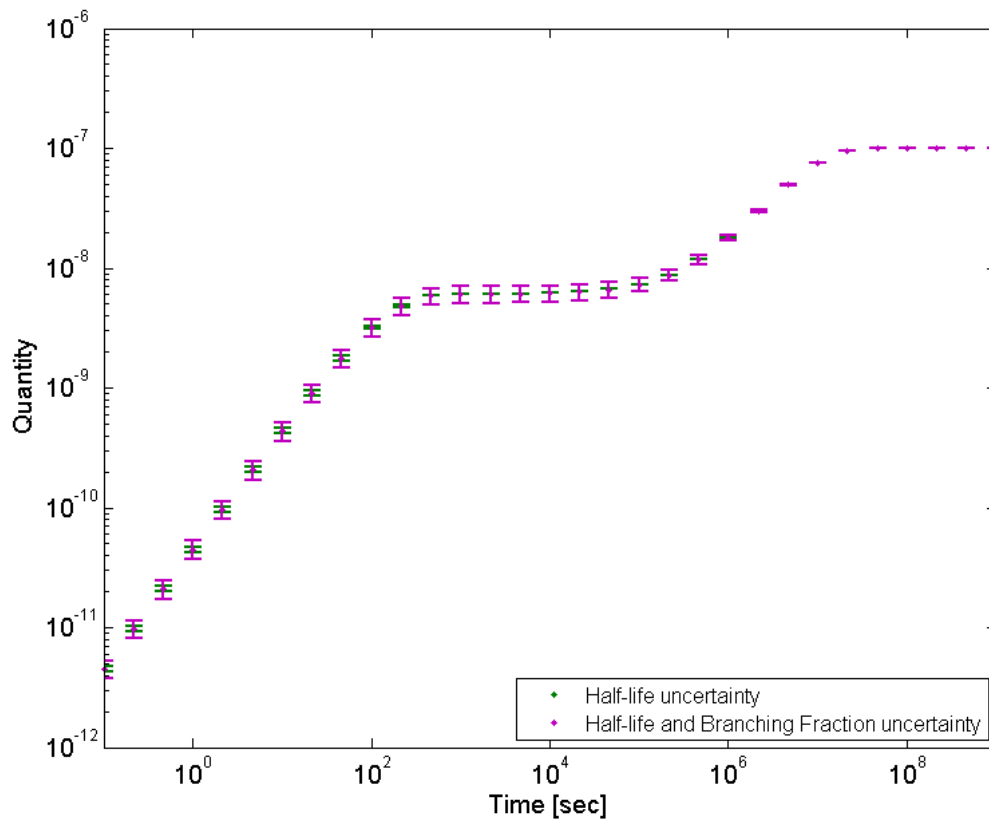
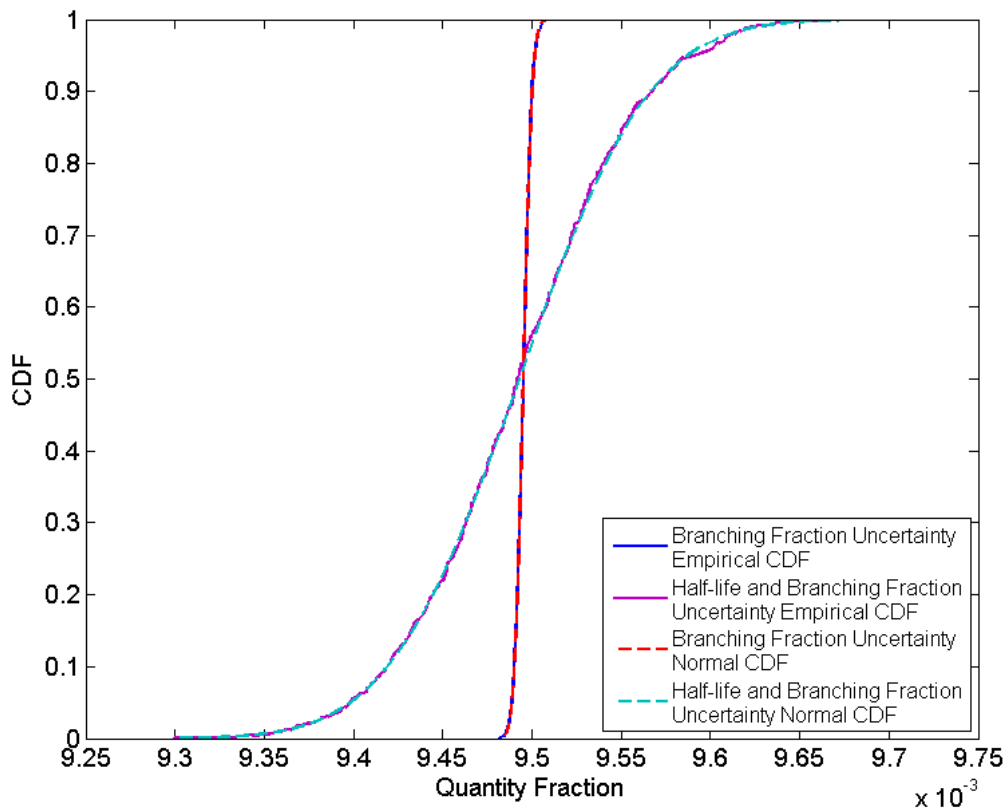


Figure 16. Log log plot of the quantity of Te124 as a function of time from Pu239 fast where  $\varphi = 20\%$ . The error bars represent one standard deviation from the mean.

The transient at early times increase the quantity by several orders of magnitude but the error bars stay within that order magnitude, and from Figure 15 the distributions remain close to normal.

The next isotope analyzed was Xe139. It was also chosen because around 100 seconds its quantity is very stable with no transients. Figure 17 shows CDFs for branching fraction compared to half-life and branching fraction uncertainty.



**Figure 17. Empirical CDFs of the Xe139 from U238 fast after 100 seconds with  $\phi = 1\%$ , as compared to a Normal CDFs with the same mean and standard deviation.**

Both the empirical and normal CDFs in Figure 17 match up very closely. They are the best fits to normal distributions thus far. When half-life uncertainty is added in it

can be seen the standard deviation and uncertainty increase significantly. This means half-life uncertainty dominates. The half-life uncertainty alone was not shown in Figure 17 because it lies directly on top of the half-life and branching fraction uncertainty CDFs. The best explanation for the Xe139 CDFs being so close to normal is that it is not going through any quantity transients.

Now an isotope that has a very large quantity uncertainty at a time needs to be examined. Figure 18 shows the quantity of Ni74 as a function of time for two runs, with only half-life uncertainty as well as half-life and branching fraction uncertainty. Branching fraction uncertainty was left out because its small error bars cluttered the plot, and added nothing.

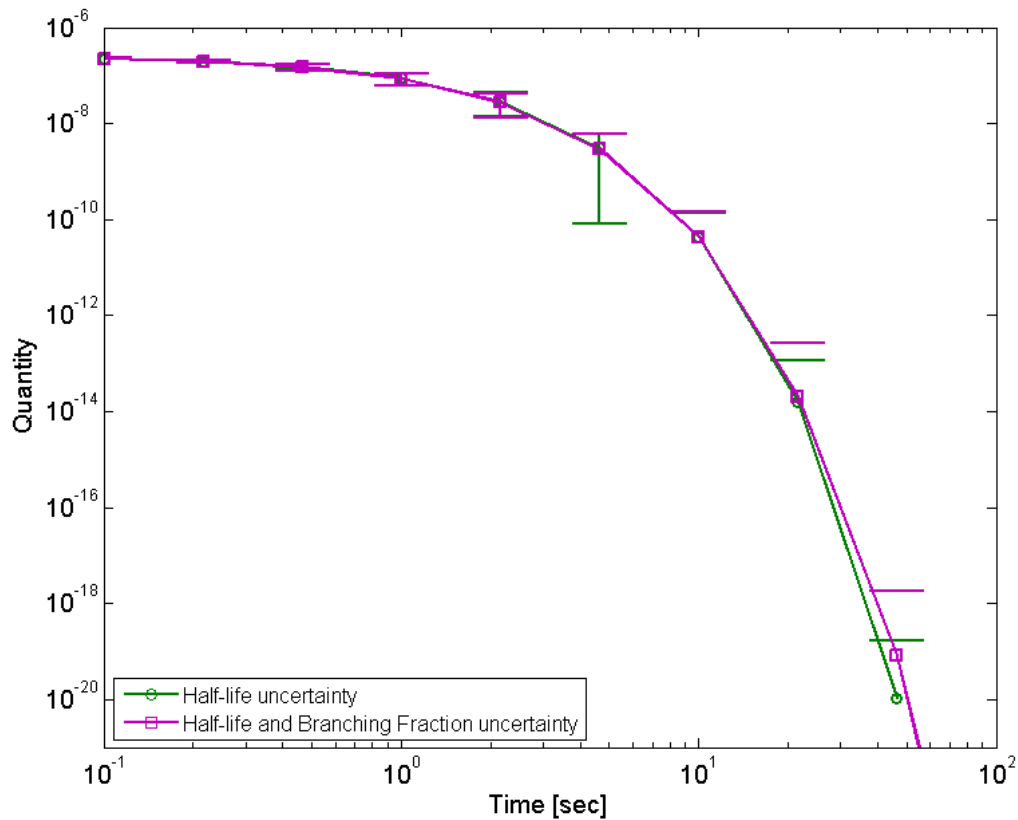


**Figure 18. Log log plot of the quantity of Ni74 as a function of time for U235 fast fission with  $\phi = 5\%$ . The error bars represent one standard deviation from the mean.**

As Ni74 begins rapidly decaying away to zero the two data sets begin to diverge. This shows how half-life uncertainty can change the quantity of a rapidly decaying isotope by orders of magnitude. This is also shown by looking at the error bars in the last three time steps where they only have an upper bound. This also corresponds to the times when its standard deviation is larger than the mean. Examining this further, Figure 19 takes a closer look at the empirical CDFs of the last time step (46.4 seconds) where this isotope is present.

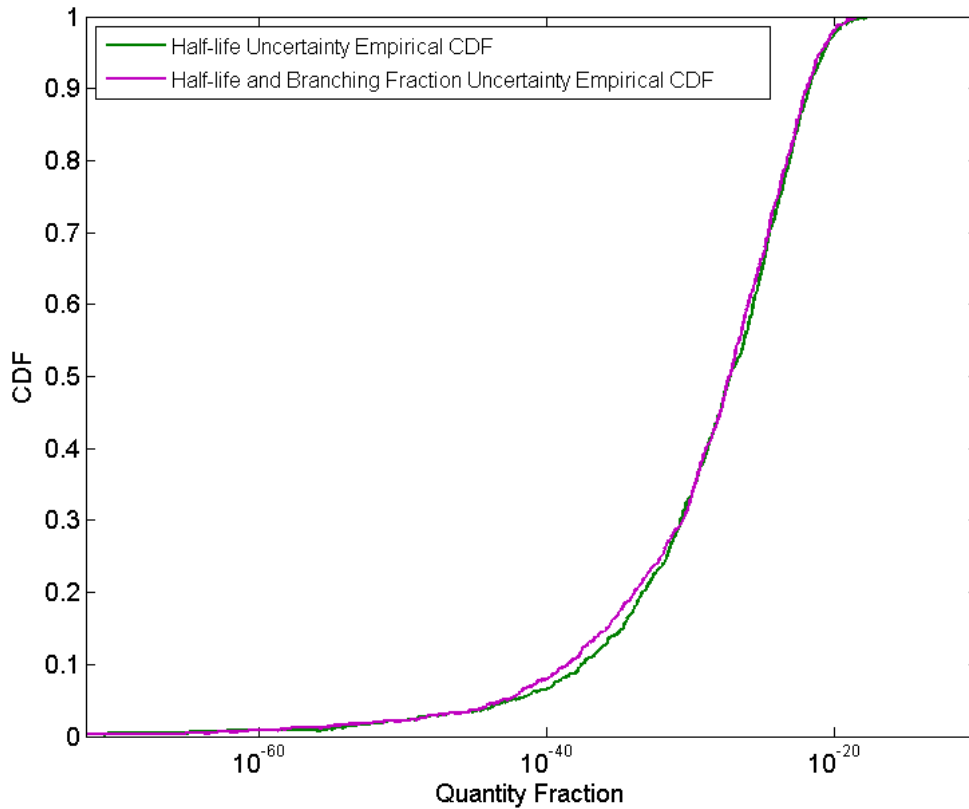


**Figure 19. Empirical CDFs of Ni74 from U235 fast fission at 46.4 seconds with  $\phi = 5\%$ .**

Note that the quantity axis in Figure 19 is logarithmic. This obviously means these distributions are not normal, but more closely follow some kind of log distribution. It also means the error bars at these late times are not accurate, and must be adjusted to accurately represent this logarithmic distribution. This was the only condition found that caused the quantity distributions to differ from normal. This condition is when half-life uncertainty is present as the isotope is decaying away rapidly to zero. The empirical CDF with only branching fraction uncertainty was also examined but again it matched a normal distribution as in the two previous example isotopes. The CDFs from an earlier time (1 second) when Ni74 is not rapidly decaying away is shown in Figure 20.



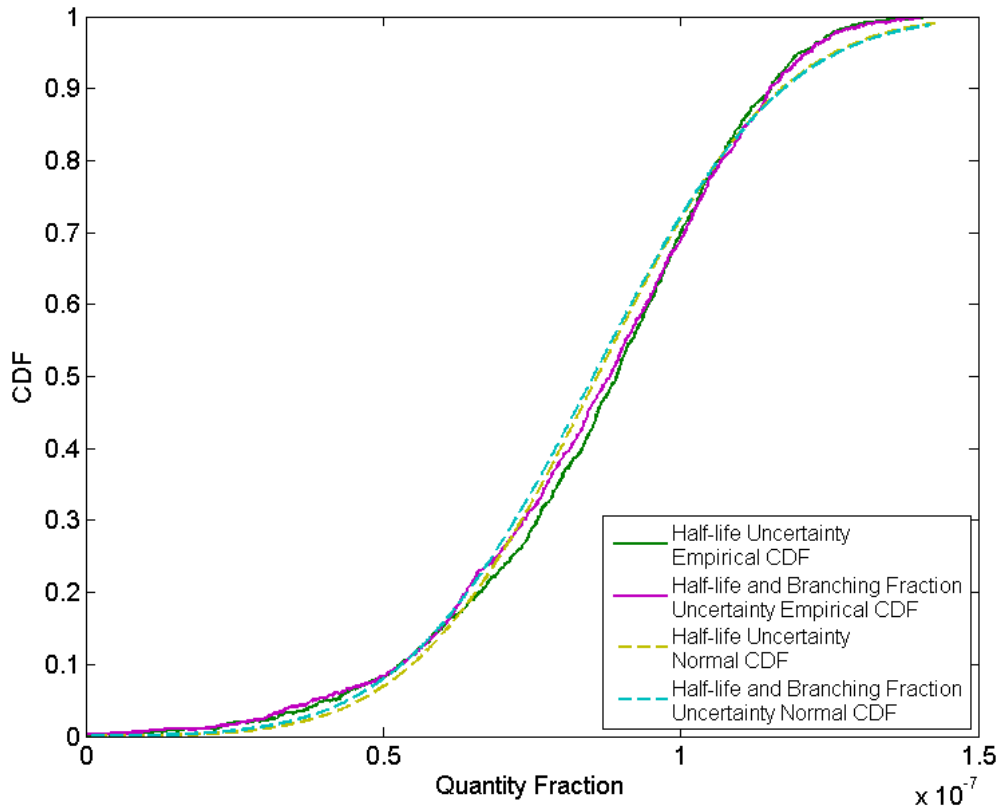


**Figure 20. Empirical CDFs of Ni74 from U235 fast at 1 second with  $\phi = 5\%$ .**

These CDFs match up much closer to normal distributions, they are at least not logarithmic. This means the error bars in Figure 18 at early times are accurate, and shows that as an isotope gets close to decaying away its quantity distribution moves to a logarithmic.

It also shows how quantity uncertainty when dominated by branching fraction uncertainty can be closely approximated by a normal distribution. This was not always the case when half-life uncertainty was dominate, especially when the isotope is rapidly decaying away.

## V. Conclusions

The objective of this study was to create a program that could be used to explore the effects of branching fraction uncertainty on radioactive decay chains. The program leveraged work already done to model half-life uncertainty using the exponential moments method and transmutation matrices. A method was developed for random sampling of branching fractions using a Dirichlet distribution marginalized by beta distributions. A sampling rejection scheme was implemented to sample these beta distributions parsimoniously and quickly.

Because branching fraction uncertainty data for most isotopes is unknown, an unbiased method for calculating uncertainties was developed. This method took the branch with the smallest mean of each isotope and made its relative standard deviation a certain percentage ( $\phi$ ). This percentage was an input parameter of the program, and was the same for all isotopes. Nine runs with 1,000 Monte Carlo trials each were completed. One run was done with only half-life uncertainty considered. Two runs were done at with  $\phi$  equal to 1%, 5%, 10%, and 20% each, one being with only branching fraction uncertainty, and the other with both half-life and branching fraction uncertainty considered.

The standard deviation from each isotope present at a given time for each of the different runs was compared. Using ratios of these uncertainties, overall uncertainty from branching fractions was compared to uncertainty due to half-lives. As a percentage of isotopes present at a given time it was shown that uncertainty due to half-lives dominated most isotopes at early times ( $< 1$  month), and uncertainty due to branching fractions

dominated at times greater than 1 month. This makes sense because half-life determines more of when an isotope is present, where branching fractions determine what amount of that isotope is present. As time passes, uncertainty due to half-life decreases while uncertainty from branching fractions increases as more decays occur introducing more opportunities for branching. Increasing  $\phi$  from 1% to 20% only increased the number isotopes dominated by branching fraction uncertainty by about 5%.

It was also shown that approximately 20% of isotopes present at any given time have uncertainties of the same order of magnitude from both half-lives and branching fractions. This means a majority of isotopes are either dominated by uncertainty from half-lives or branching fractions. When only isotopes present in greater quantities are considered, the percent of isotopes present dominated by branching fractions increases at times later than 1 minute.

The quantity distributions about the means can be considered very close to normal regardless of if uncertainty due to half-life or branching fraction dominates. The only known exception to this is when an isotope begins rapidly decaying to zero on a log time scale. As this occurs the distribution becomes logarithmic.

This study only looked for general guidelines that can be applied. The program is flexible and the data outputs sufficient enough to study particular chains or isotopes of interest to get a better idea of branching uncertainty effects on them.

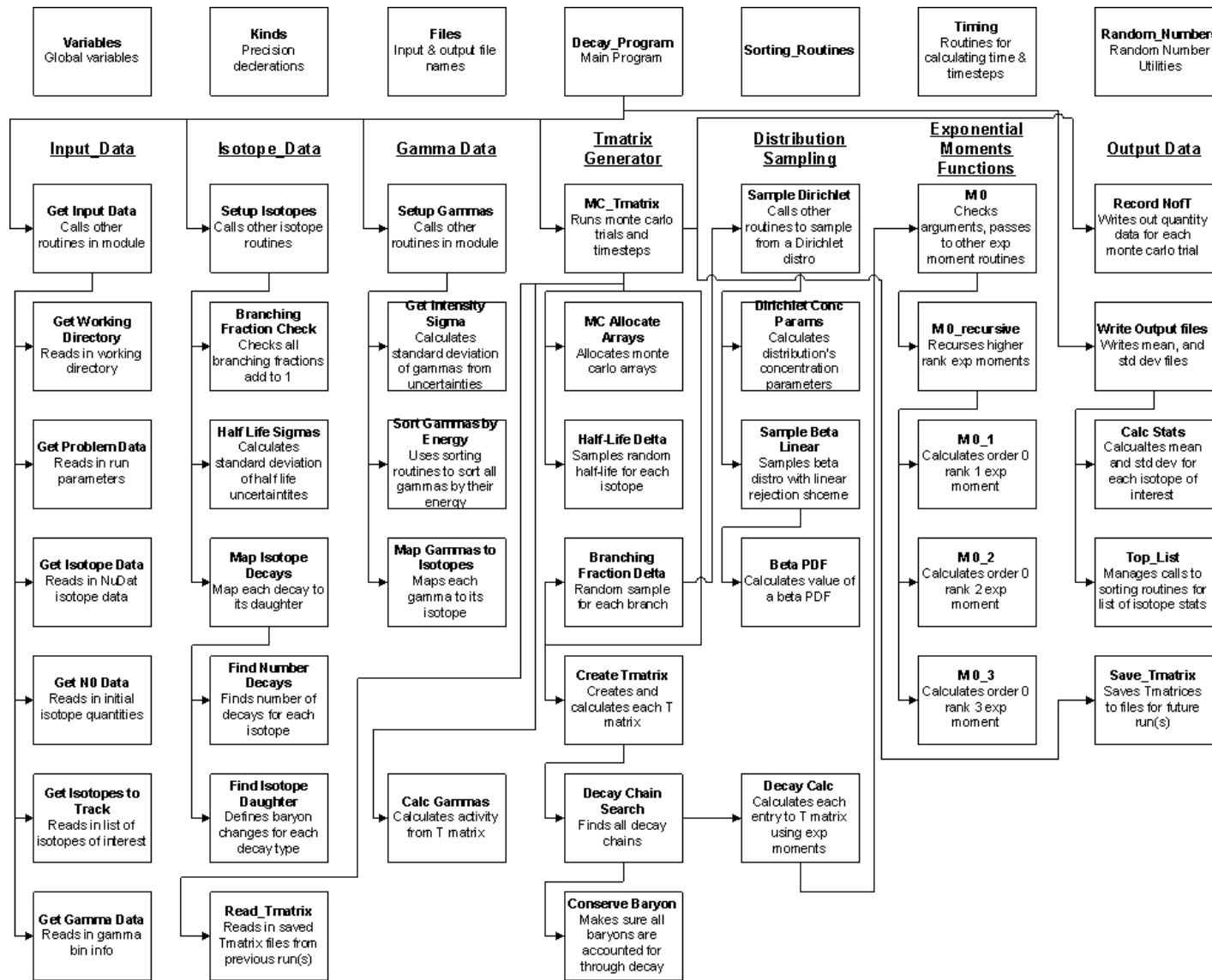
### **Potential Future Work**

It should be remembered that this work was only a parameter study, with all the branching fraction uncertainties being applied in a somewhat equitable manner. The

most logical improvement to the program would be to use experimentally determined branching fraction uncertainty data. If enough of these data become available to incorporate, it should be remembered that if the variance of one of the branches for an isotope is known, the variance of the other branches is already determined. This means if variances for multiple branches are experimentally determined, a method for weighting each dataset must be developed so as to give an accurate Dirichlet distribution. Another improvement would be to include uncertainty of the initial quantity of isotopes from neutron induced fission. If this is done, it should be remembered this can also be represented with a Dirichlet distribution because it is categorical. However the Dirichlet distribution will have many more parameters, upwards of 821, with the potential for very large parameters that could not be randomly sampled with double machine precision.

Improvements to the efficiency of the program are another area for future work. These include saving out the all the decay chains to an array so they would not have to be calculated each Monte Carlo run, or a more parsimonious way of sampling the half-life uncertainty distributions.

Appendix A: Design Diagram of Decay Program



## Appendix B: Derivation of Standardized Beta pdf

Probability density function for a beta distribution with parameters  $\alpha$  and  $\beta$ .

$$\text{Beta}(x; \alpha, \beta) = \frac{x^{\alpha-1}(1-x)^{\beta-1}}{B(\alpha, \beta)} \quad (23)$$

$$\text{where } B(\alpha, \beta) = \int_0^1 t^{\alpha-1}(1-t)^{\beta-1} dt$$

$$\text{let } a = \alpha - 1, \text{ and } b = \beta - 1$$

with a domain of  $a > 0$ ,  $b > 0$ , and  $0 < x < 1$

The beta distribution pdf is now:

$$\text{Beta}(x; a, b) = \frac{x^a(1-x)^b}{B(a+1, b+1)} \quad (24)$$

To standardize the pdf the max value must be known (where the peak is), this is done by finding where the derivative with respect to  $x$  is equal to zero.

$$\text{Beta}'(x; a, b) = \frac{(1-x)^{b-1}x^{a-1}(a(1-x) - bx)}{B(a+1, b+1)} = 0 \quad (25)$$

The only way Equation (25) can be equal to zero is when  $(a(1-x) - bx) = 0$ . Solve for  $x$ :

$$x = \frac{a}{a+b} = \frac{\alpha-1}{\alpha+\beta-2} \quad (26)$$

this equation is equal to the mode of a Beta distribution.

Now the pdf can be standardized to a peak value of one by dividing by the peak value.

$$\frac{\text{Beta}(x; a, b)}{\text{Beta}\left(\frac{a}{a+b}; a, b\right)} = \left(\frac{(a+b)(1-x)}{b}\right)^b \left(\frac{(a+b)x}{a}\right)^a \quad (27)$$

This is a fairly simple equation that is not only standardized to a peak value of one, but also does not have a Beta function in it. It can be further simplified to:

$$\text{Beta}_S(x; a, b) = \frac{(a + b)^{a+b}}{a^a b^b} x^a (1 - x)^b \quad (28)$$

The issue with Equations (27) and (28) is that when either  $a$ ,  $b$ , or  $a + b$  get large they can numerically overflow. This is resolved by taking the log of each side and leveraging logarithm rules so Equation (28) becomes:

$$\text{Beta}_S(x; a, b) = e^{(a+b)\log(a+b) - a\log(a) - b\log(b) + a\log(x) + b\log(1-x)} \quad (29)$$

### Appendix C: Derivation of Beta pdf Inflection Points

Take either Equation (27) or (28) and find its second derivative.

$$\text{Beta}_S''(x; a, b) = \frac{\left(\frac{(a+b)(1-x)}{b}\right)^b \left(\frac{(a+b)x}{a}\right)^a (a^2(x-1)^2 + (b-1)bx^2 + a(x-1)(1+(2b-1)x))}{(x-1)^2x^2} \quad (30)$$

The inflection points are where the second derivative is equal to zero. The only way for this to happen in Equation (30) is for the third factor to be equal to zero.

$$(a^2(x-1)^2 + (b-1)bx^2 + a(x-1)(1+(2b-1)x)) = 0$$

Solve for  $x$ :

$$x = \frac{a^2 + a(b-1) \pm \sqrt{ab(a+b-1)}}{a^2 + (b-1)b + a(2b-1)} \quad (31)$$

If  $a \leq 1$  or  $b \leq 1$ , then one or both inflection points will be outside  $x$ 's range of  $(0,1)$ . If this is the case then the rejection scheme only uses the relative slope points and the constant around the peak of the standardized pdf. As  $a$  and  $b$  approach one in the minus case, loss of precision occurs. This is taken care of by multiplying Equation (31) by:

$$x = \left( \frac{a^2 + a(b-1) - \sqrt{ab(a+b-1)}}{a^2 + (b-1)b + a(2b-1)} \right) \left( \frac{a^2 + a(b-1) + \sqrt{ab(a+b-1)}}{a^2 + a(b-1) + \sqrt{ab(a+b-1)}} \right)$$

If the numerator and denominator are expanded and terms cancelled Equation (32) is the result.

$$x = \frac{a^2 - a}{a^2 + a(b-1) + \sqrt{ab(a+b-1)}} \quad (32)$$

Equation (32) is now well-conditioned and can be used for the minus case of Equation (31).



## Appendix D: Derivation of Inverting CDF for a line

For a line  $s$  with a left bound of  $x_0$  and right bound of  $x_1$ , let  $s(x_0) = s_0$ ,  $s(x_1) = s_1$  then the equation for the line is:

$$s(u) = s_0(1 - u) + s_1u \quad (33)$$

$$\text{where } u = \frac{x - x_0}{x_1 - x_0}$$

$$\text{and } 0 \leq u \leq 1$$

Integrate Equation (33) to get the total area under the line.

$$\int_0^1 s(u) du = \frac{s_0 + s_1}{2} \quad (34)$$

Then divide the equation for the line by Equation (34) and integrate to get its CDF.

$$\int_0^u \frac{2s(u)}{s_0 + s_1} du = \frac{2s_0u - s_0u^2 + s_1u^2}{s_0 + s_1} \quad (35)$$

Set Equation (35) equal to  $\zeta$ , a random number between  $[0,1)$  and solve for  $u$ .

$$u(\xi) = \frac{s_0 \pm \sqrt{s_0^2 - s_0^2\xi + s_1^2\xi}}{s_0 - s_1} \quad (36)$$

To find the correct root solve  $u(1)$ , and  $u(0)$  for each case. For the plus case  $u(0) =$

$$\frac{2s_0}{s_0 - s_1}, u(1) = \frac{s_0 + s_1}{s_0 - s_1}, \text{ for the minus case } u(0) = 0, u(1) = 1. \text{ The minus case is correct}$$

for the CDF. Expanding Equation (36) and factoring to remove the  $s_0 - s_1$  from the denominator results in:

$$u(\xi) = \frac{(s_0 + s_1)\xi}{s_0 + \sqrt{s_0^2(1 - \xi) + s_1^2\xi}} \quad (37)$$

The  $(1 - \xi)$  in the denominator will not result in loss of precision because  $\xi$  lives in  $[0,1)$ . Now  $u$  can be randomly sampled from the CDF of the line  $s$ . Because of the method developed with four linears and a constant two of the sampling function lines will have either  $s_0 = 0$ , or  $s_1 = 0$ . When  $s_0 = 0$ , Equation (37) simplifies to  $\sqrt{\xi}$ , and when  $s_1 = 0$  it simplifies to  $\xi/(1 + \sqrt{1 - \xi})$ .

## Appendix E: Derivation of Standardized Beta pdf Relative Slope

Start with either Equation (27) or (28) from Appendix B, and taking its derivative you get an equation for the slope of the standardized beta pdf:

$$\text{Beta}_S'(x; a, b) = \frac{\left(\frac{(a+b)(1-x)}{b}\right)^b \left(\frac{(a+b)x}{a}\right)^a (a(1-x) - bx)}{(1-x)x} \quad (38)$$

Then divide the slope by the standardized pdf to get the relative slope.

$$\frac{\text{Beta}_S'(x; a, b)}{\text{Beta}_S(x; a, b)} = S_R = \frac{a(x-1) + bx}{(x-1)x} = \frac{a}{x} + \frac{b}{(x-1)} \quad (39)$$

where  $S_R$  is the relative slope. Solving for  $x$  results in two solutions:

$$x = \frac{a + b + S_R \pm \sqrt{(a + b + S_R)^2 - 4aS_R}}{2S_R} \quad (40)$$

of which the minus is correct because it yields solutions within the domain  $0 < x < 1$ .

## Appendix F: Prioritized List of Model and Code Improvements

1. Parallelization: Because the program relies on Monte Carlo methods, there is great potential that parallelization could reduce runtimes. However the auto parallelization feature in the Intel compiler actually increased runtimes. An analysis of the code by someone experienced in parallelization techniques is needed. With today's multi-processor computers this could lead to the greatest reduction in runtime.
2. Incorporate known branching fraction uncertainties: Some branching fraction uncertainties are documented, and more may be done in the future. A method that incorporates these uncertainties while still adhering to the model laid out in this study is needed.
3. Calculate decay chains only once: Currently decay chains for all the isotopes are calculated for each time of each Monte Carlo trial. These decay chains do not change, making this method redundant. The large number of decay chains may make it infeasible to save to an array, or too inefficient to write to a file and read back in every time. However, these or other methods need to be explored for efficiency sake.
4. Improve sampling of half-life uncertainties: The method used is not parsimonious in random numbers, and is not realistic for a Gaussian distribution (when an isotope is quoted as having a  $+\sigma$  and  $-\sigma$ ). It was recommended by NIST

to splice the two halves of the different Gaussians together. If this is done you get a distribution similar to the one in Figure 21.

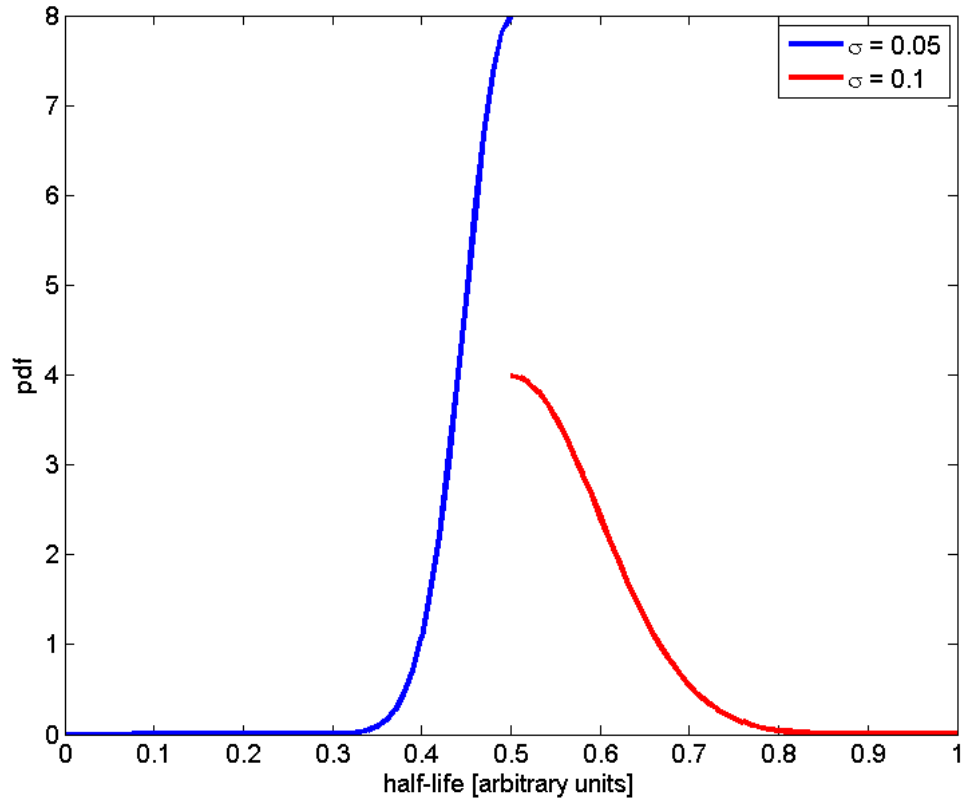


Figure 21. pdf of two Gaussians with different standard deviations spliced together. The mean is 0.5.

Approximately 200 isotopes in the current NuDat data have two different  $\sigma$  values. A more appropriate distribution is needed that does not have a step value at the mean, and satisfies both  $\sigma$  values.

5. Incorporate uncertainty in initial quantities: This is another piece in the physics of radioactive decay that needs to be explored as a significant source of uncertainty. As an example fission fragment yields range across many orders of magnitude ( $10^{-2}$  to  $10^{-14}$ ). Because of this, uncertainty in these yields could have an impact in decay isotope quantities.
6. Account for spontaneous fission: For this study the fraction of an isotope that can spontaneously fission was ignored. This could be done because no isotopes that result from neutron induced fission can spontaneously fission. This does need to be accounted for to make the code complete.
7. Improve the Beta distribution rejection scheme: The current rejection scheme has an average acceptance rate of around 63%. If the goal of the user is run more Monte Carlo trials and only a few times, then improving this scheme would result in a noticeable reduction in runtime.
8. Transmutation matrix inversion: Inverting the T-matrices would allow the user to calculate quantities present at earlier times with uncertainty. This is useful in nuclear forensics, where the quantity of an isotope is measured at a time after a nuclear event. The need is to be able to plug this amount into a program that will give the isotopes initially present with uncertainty.

## Bibliography

- [1] L. J. Harr, Precise Calculations of Complex Radioactive Decay Chains, 2007.
- [2] "NuDat 2.6," National Nuclear Data Center, Brookhaven National Laboratory, [Online]. Available: <http://www.nndc.bnl.gov/nudat2/>. [Accessed November 2012].
- [3] S. Kotz, N. Balakrishnan and N. L. Johnson, Continuous Multivariate Distributions, Volume 1: Models and Applications, Second Edition, John Wiley & Sons, 2000.
- [4] K. A. Mathews, "Random Sampling from the Klein-Nishina Distribution: Efficiency, Parsimony, and Speed," Draft 2012.
- [5] T. R. England and B. F. Rider, "Evaluation and Compilation of Fission Product Yields," LA-UR-94-3106, ENDF-349, October 1994.
- [6] C. J. Bridgman, Introduction to the Physics of Nuclear Weapon Effects, 2001.
- [7] Knolls Atomic Power Laboratory, Nuclides and Isotopes, Chart of the Nuclides, Seventeenth Edition, 2009.
- [8] S. J. Chapman, Fortran 95/2003 for Scientist and Engineers, 3rd Edition, 2004.
- [9] K. A. Mathews, "Exponential Moment Methods: Mathematics, Fortran, Algorithms, Codes," Draft 2012.
- [10] K. A. Mathews, *Personal Communication*. September-December 2012.

## REPORT DOCUMENTATION PAGE

*Form Approved*  
*OMB No. 074-0188*

The public reporting burden for this collection of information is estimated to average 1 hour per response, including the time for reviewing instructions, searching existing data sources, gathering and maintaining the data needed, and completing and reviewing the collection of information. Send comments regarding this burden estimate or any other aspect of the collection of information, including suggestions for reducing this burden to Department of Defense, Washington Headquarters Services, Directorate for Information Operations and Reports (0704-0188), 1215 Jefferson Davis Highway, Suite 1204, Arlington, VA 22202-4302. Respondents should be aware that notwithstanding any other provision of law, no person shall be subject to any penalty for failing to comply with a collection of information if it does not display a currently valid OMB control number.

**PLEASE DO NOT RETURN YOUR FORM TO THE ABOVE ADDRESS.**

<b>1. REPORT DATE (DD-MM-YYYY)</b> 21 Mar 2013			<b>2. REPORT TYPE</b> Master's Thesis		<b>3. DATES COVERED (From - To)</b> Sep 2011 - Mar 2013	
<b>4. TITLE AND SUBTITLE</b> Modeling Radioactive Decay Chains with Branching Fraction Uncertainties				<b>5a. CONTRACT NUMBER</b>		
				<b>5b. GRANT NUMBER</b>		
				<b>5c. PROGRAM ELEMENT NUMBER</b>		
<b>6. AUTHOR(S)</b> Higley, Timothy M., Captain, USAF				<b>5d. PROJECT NUMBER</b> N/A		
				<b>5e. TASK NUMBER</b>		
				<b>5f. WORK UNIT NUMBER</b>		
<b>7. PERFORMING ORGANIZATION NAMES(S) AND ADDRESS(S)</b> Air Force Institute of Technology Graduate School of Engineering and Management (AFIT/EN) 2950 Hobson Way WPAFB OH 45433-7765				<b>8. PERFORMING ORGANIZATION REPORT NUMBER</b> AFIT-ENP-13-M-14		
<b>9. SPONSORING/MONITORING AGENCY NAME(S) AND ADDRESS(ES)</b> Dr. David W. Gerts Air Force Technical Applications Center 1030 S. Highway A1A Patrick AFB, FL 32925 (321)494-7336, DSN: 854-7336				<b>10. SPONSOR/MONITOR'S ACRONYM(S)</b> AFTAC/THD		
				<b>11. SPONSOR/MONITOR'S REPORT NUMBER(S)</b>		
<b>12. DISTRIBUTION/AVAILABILITY STATEMENT</b> DISTRIBUTION STATEMENT A. APPROVED FOR PUBLIC RELEASE; DISTRIBUTION UNLIMITED						
<b>13. SUPPLEMENTARY NOTES</b> This material is declared a work of the U.S. Government and is not subject to copyright protection in the United States.						
<b>14. ABSTRACT</b> This thesis is a parameter study of the effects of branching fraction uncertainty from nuclear decay on isotope quantities at later times. Development of how to calculate and accurately draw random samples of branching fractions is done. Overall effects as well as isotope quantity uncertainty distributions are also explored. Isotope quantities are calculated using exponential moments methods with transmutation matrices. Uncertainty from both half-lives and branching fractions is carried through these calculations by Monte Carlo methods. Results of the study show that uncertainty from branching fractions dominates most isotopes present from neutron fission after approximately one month. Another result is that only 20% of isotopes present at any given time have uncertainty from both half-lives and branching fractions that are of the same order of magnitude. The final program is both flexible in the number and type of isotopes it can input and output, as well as computationally efficient.						
<b>15. SUBJECT TERMS</b> Branching Fractions, Half-life, Uncertainty, Radioactive Decay Chains, Exponential Moments						
<b>16. SECURITY CLASSIFICATION OF:</b>			<b>17. LIMITATION OF ABSTRACT</b>	<b>18. NUMBER OF PAGES</b>	<b>19a. NAME OF RESPONSIBLE PERSON</b>	
<b>a. REPORT</b>	<b>b. ABSTRACT</b>	<b>c. THIS PAGE</b>			Mathews, Kirk A., Ph.D, AFIT/ENP	
U	U	U	UU	87	<b>19b. TELEPHONE NUMBER (Include area code)</b> (937)255-3636, ext. 4508	

Standard Form 298 (Rev. 8-98)  
Prescribed by ANSI Std. Z39-18